Mountain Home Geothermal Area: Preliminary Natural State Model

Sabodh K. Garg

Technical Report

Leidos, Inc.
10260 Campus Point Drive
San Diego, CA 92121

Submitted to:
Utah State University
4505 Old Main Hill
Logan, Utah 84322

August 2015

I. Background

Under a co-operative agreement with the U.S. Department of Energy (DOE), Utah State University is carrying out a research program to identify promising geothermal prospects in the Snake River Plain (SRP) volcanic province. The goals of this Phase 1 study are to: (1) adapt the methodology of *Play Fairway Analysis* for geothermal exploration, creating a formal basis for its application to geothermal systems, (2) assemble relevant data for the Snake River Plain volcanic province from publicly available and private sources, and (3) build a geothermal play fairway model for the Snake River Plain that will allow the delineation of the most promising plays, using software tools that are standard in the petroleum industry. The model will serve to integrate the diverse data sets and serve as a point of departure for future exploration efforts in the region. A promising play type is associated with the SRP basaltic sill-complexes characterized by fault-controlled permeability, volcanic sill heat source, and lake sediment seal. The area around Mountain Home Air Force base in western Snake River Plain (Figure 1) hosts a geothermal system of the latter type.

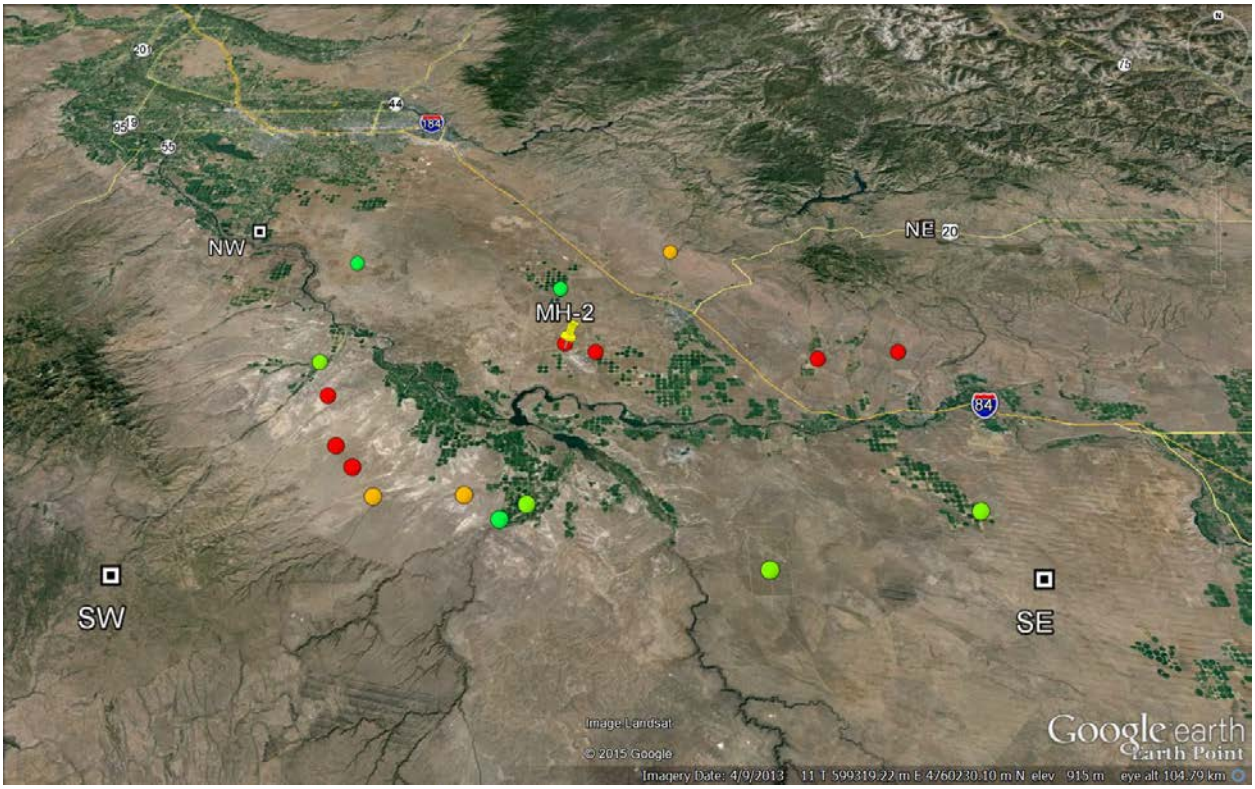

Figure 1: Mountain Home area showing the locations of boreholes greater than 200 meters in depth. The NW (Lat: 43.31, Long: -116.51), NE (43.31, -115.19), SW (42.71, -116.50), ad SE (42.71, -115.20) denote the four corners of the area of interest.

The Mountain Home area is characterized by high heat flow and temperature gradient. Temperature data are available from 18 boreholes (Figure 1) with depths equal to or greater than 200 m; although there are large variations, the average temperature gradient exceeds 80^{o}C/km. This report presents a preliminary 3-D numerical model of the natural-state (i.e. pre-production state) of the Mountain Home geothermal area conditioned using the available temperature profiles from the five deep wells with depths ranging from ~1340 m to ~3390 m (MH-1, MH-2, Bostic1, Lawrence D No.1, and Anschutz No. 1); the preliminary natural state model will be further developed during Phase 2 as additional geological, geophysical, and well data become available.

II. Numerical Model – an Introduction

A hydrothermal system such as the Mountain Home geothermal prospect contains a convecting fluid mixture that is heated at depth and then rises towards the surface as a consequence of buoyancy. The system is not only nonisothermal but is also in a continuous state of flow. The development of a natural-state model requires a variety of geological, geophysical, geochemical and hydrological data sets. A computer based simulation of the natural fluid and heat flow in the geothermal reservoir offers the framework for synthesizing these evolving data sets (*i.e.,* presumably as a result of drilling and production/injection operations) into an integrated geohydrological model. Such natural-state modeling also helps in the evolution of the conceptual model by revealing inconsistencies and physical shortcomings in the preliminary conceptual model of the reservoir.

Assessment of the natural-state model is usually carried out by comparing theoretical predictions of quantities such as reservoir pressure and temperature, and surface heat and mass discharge with field measurements. This process very often provides insight into reservoir parameters such as formation permeability distribution, and boundary conditions for heat and mass recharge at depth. The natural-state model can also be used to evaluate the effects of gaps in the available data base on future reservoir performance. Planning of future drilling and well tests for reservoir verification could then be based on resolving major uncertainties in the evolving model for the geothermal reservoir. For fields which have not yet been exploited, or have been in operation for only a few years, the natural-state information comprises the bulk of the data available for reservoir modeling.

It is not sufficient to merely prescribe a “natural state” based, for example, upon interpolation between measured, or inferred, pressures and temperatures. It is essential, in fact, that the natural state itself represents a quasi-steady solution of the partial differential equations that govern flow in the reservoir. Otherwise, solution of the production/injection phase of the problem is likely to produce changes in underground pressures and temperatures that are unrelated to exploitation, but are instead fictitious consequences of the initial (*i.e.*, pre-production or natural) conditions being inconsistent with steady behavior. Since transient processes associated with initiation of convection occur over time scales of the order of 10^4 to 10^5 years, the natural state can be regarded as stationary over the 10–50 year period required to exploit a geothermal reservoir. Thus, the requirement that the natural state be itself a nearly steady solution of the governing equations is an essential test of the model of the reservoir.

A definite volume must be chosen for a computer simulation of the reservoir system. For modeling purposes, it is useful to visualize the reservoir as a region of hot water surrounded by cold water on the sides. The reservoir boundaries are usually diffuse and irregular because of variations in formation properties such as permeability; for the sake of simplicity, the boundaries are assumed to have simple geometrical shapes. At the margins of the field, there are inflows of cold water and outflows of hot water and the temperature pattern is complicated. Inside the reservoir itself, cold- water recharge from the top and/or sides will mix with the hot water inflow from the base and produce spatial variations in the fluid state.

Determination of the natural state amounts to solving an inverse problem, and is accomplished by a procedure amounting to successive approximation. The quasi-steady (or stationary) state depends mainly upon the boundary conditions imposed upon the perimeter of the system volume (such as pressures, temperatures, and deep heat flux and hot fluid sources) and upon the distributions of formation properties (such as porosity and permeability) believed to prevail within it. Thus, given estimates of the boundary conditions and formation properties, the corresponding stable state is found. This solution may be examined to see how well it matches known facts about the system (such as measured downhole pressures, temperatures, fluid state, advective zones within the reservoir and distribution of surface discharge). Appropriate adjustments are then made in the boundary conditions and/or formation properties in an effort to improve agreement between measurements and computed results, and the problem is solved again. In this way, the natural state is found in an iterative fashion involving repetitive calculations of the pseudo-steady state.

The pseudo-steady states are usually computed by carrying out a time-dependent calculation representing thousands of years of physical evolution of the reservoir. A fundamental conceptual problem exists in the selection of the boundary conditions and the initial conditions. During the thousands of years required for the evolution of the reservoir to its present state, the boundary conditions themselves must have undergone change. Thus, for example, heat transfer from a magma intrusion is at a maximum just after its emplacement, and declines (exponentially?) with time. We have, of course, no way of determining the evolution of boundary conditions with time, and must perforce employ time invariant boundary conditions. These time invariant boundary conditions are usually chosen to represent the present day situation. The time dependent calculation does not, therefore, strictly represent the actual physical evolution of the system; it is rather an attempt to mimic the evolution of the geothermal system to its present state using a mathematically tractable model. As far as the specification of initial conditions is concerned, the problem is somewhat simpler. The influence of the initial conditions upon the solution declines as time goes on and, in principle, becomes exactly zero when a steady state is reached. Therefore, the exact details of the initial conditions are relatively unimportant. All that is required for initial conditions is a state that is (1) physically plausible and (2) consistent with the applied boundary conditions.

Despite the fact that (as noted above) the calculation of the evolution of the system to the natural state does not exactly replicate the true evolution over time due to the necessity of imposing constant boundary conditions and fixed formation property distributions and to uncertainties concerning the exact initial state, the time-duration of the natural-state calculation should bear some resemblance to reality. The typical ages of geothermal systems vary from ~10^4 to ~10^6

years, but in tectonically active volcanic regions such systems are unlikely to remain unchanged for over ~10^5 years or so. This means that the system will never reach an exactly steady condition since the time required for thermal conduction processes (the slowest heat transfer mechanism) to reach equilibrium will normally be much longer. Generally speaking, natural-state calculations usually represent between 10^4 and 10^6 years; the resulting state, while not exactly steady, will be characterized by changes that are imperceptible on time-scales of centuries. As such, they comprise appropriate starting conditions for modeling reservoir exploitation.

III. Computational Volume, Model Grid, Formation Properties, and Boundary Conditions

The ground surface elevation in the Mountain Home area varies from about 690 mASL (meters above sea-level) to over 2200 mASL. The bottom of the deepest well drilled so far Anschutz 1 is at about -2555 mASL. It was, therefore, decided to place the bottom of the model grid at 3000 m below sea-level; thus the model grid extends about 450 m below the deepest well. The top of the model grid is placed at the assumed water level (1 bar surface).

At present, no pressure transient data are available from any of the wells in the Mountain Home area. The vertical permeability values were determined during the development of the numerical model in order to match the measured well temperatures. The horizontal permeability values in the model are largely unconstrained. In the future, permeability values used in the model will be modified as additional geological, geophysical, and well test data become available.

The model volume is divided in to a 22x16x18 grid in the x- and y- and z-directions (east, north, and vertically upwards) respectively. In the z-direction, the grid blocks are either 100 m or 250 m. In the x- and y-directions, a uniform grid spacing of 5 km was employed. The total number of the grid blocks is 6336, and the model volume is 34,320 cubic kilometers (110 km in the east-west direction, 80 km in the north-south direction, and 3.9 km in the vertical direction). An overlay of the horizontal grid over the Mountain Home area is shown in Figure 2. The vertical grid is displayed in Figure 3.

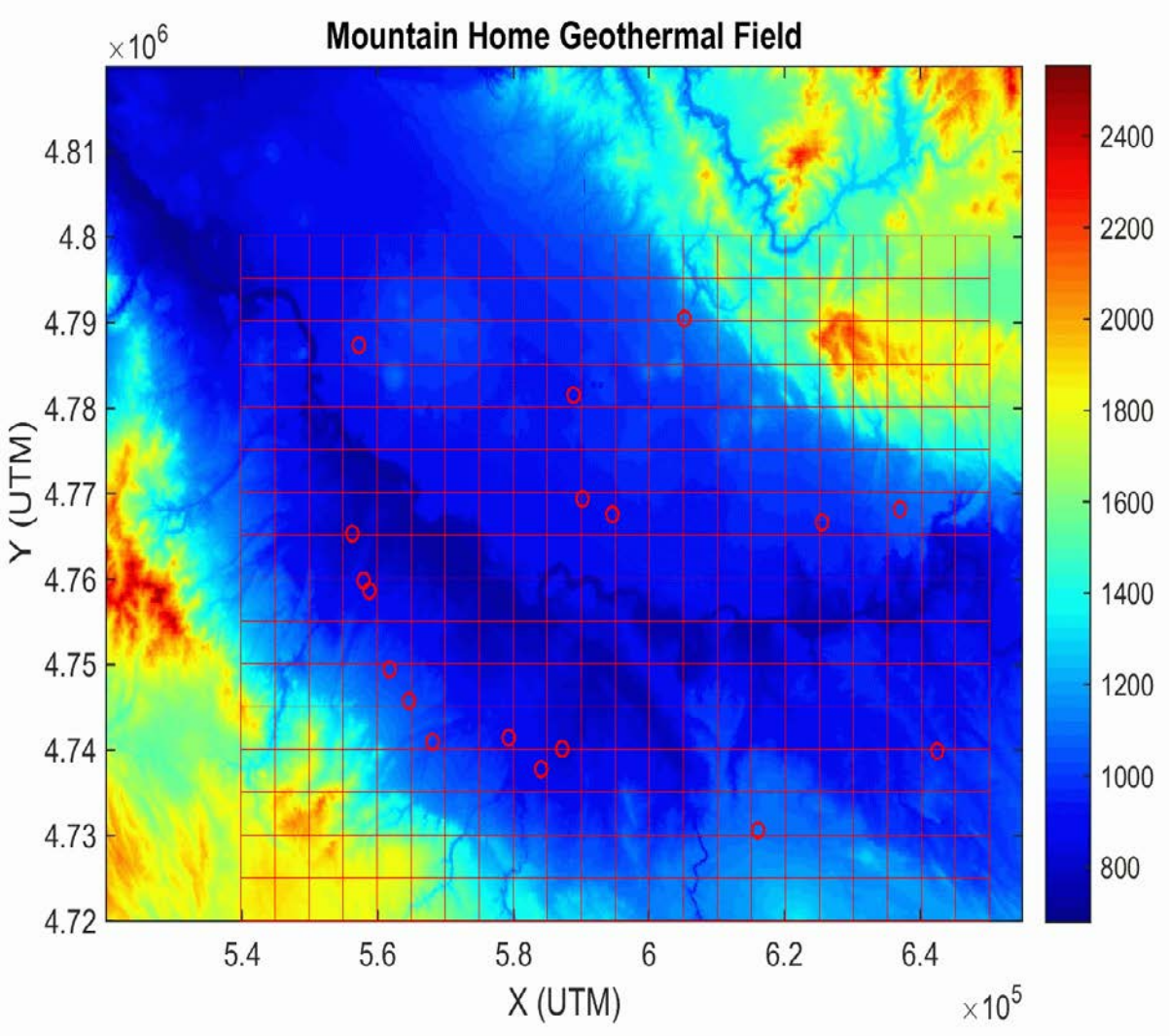

Figure 2: Horizontal grid (x-y grid) superposed on a topographic map of the Mountain Home geothermal prospect; warm colors denote higher elevations. Well-heads (red circles) are also shown. The origin of the model grid is at 540,000 mE and 4,720,000 mN (UTM).

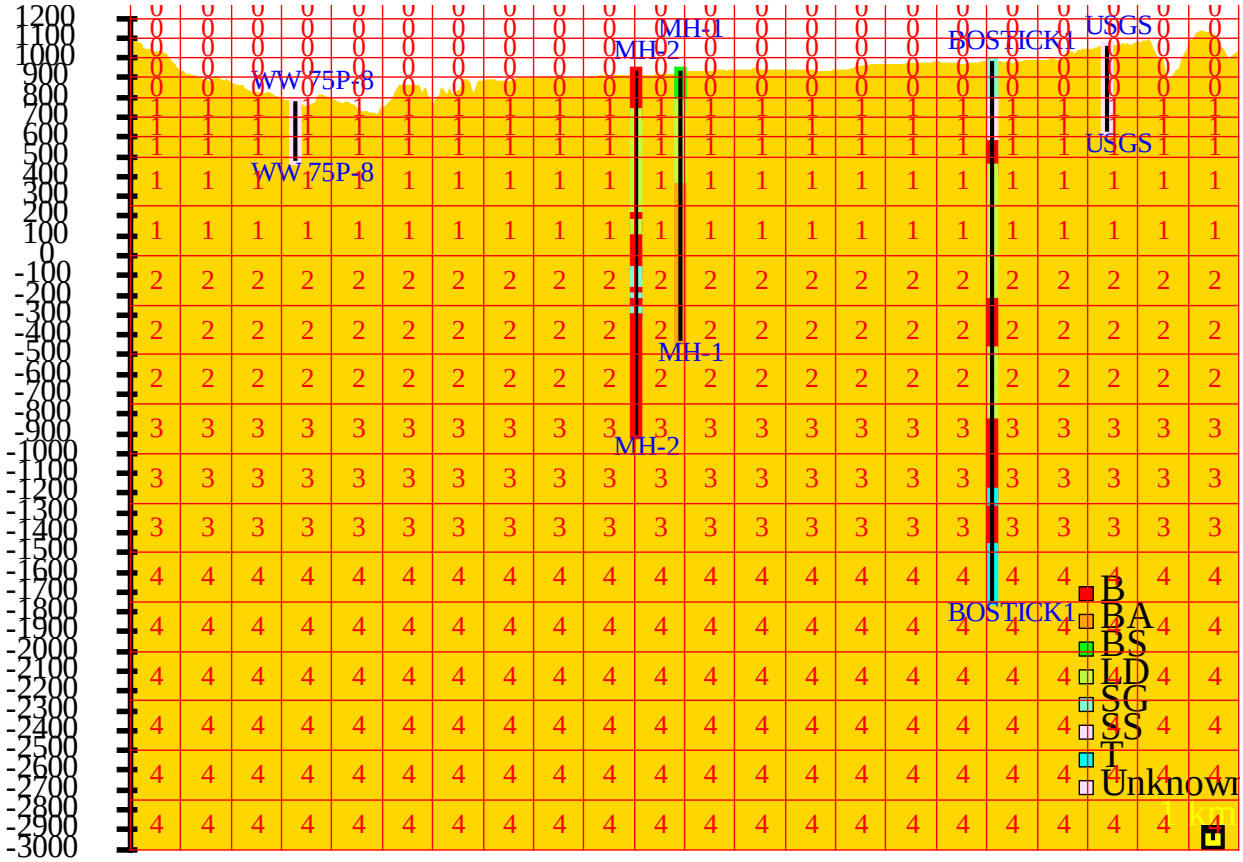

Figure 3: Vertical (x-z) model grid at y= 47.5 km (j=10). The bottom of the grid is at -3000 mASL. The bottom 14 grid blocks (k=1 to 14) are of uniform thickness (250 m each); a smaller thickness (100 m) is used for blocks k=15 and higher in order to more closely represent the water level surface. Numbers in grid-blocks (1, 2, 3, and 4) denote the formation type (see below). The void blocks are tagged with 0. Also shown is the lithology from the deep wells (MH-1, MH-2, and Bostic1) passing through j=10.

The 3-D numerical model was constructed using Leidos's STAR geothermal reservoir simulator (Pritchett, 2011). In order to carry out model computations with STAR (or for that matter any other reservoir simulator), it is essential to prescribe distribution of thermo-hydraulic properties (*e.g.*, permeability, porosity, thermal conductivity, specific heat, etc.) for the entire grid-volume, and boundary conditions along the faces of the model grid. During the development of the natural-state model for the Mountain Home geothermal prospect presented below, the boundary conditions (*i.e.*, heat flux along the bottom boundary, pressure specification along the top boundary) and the formation permeabilities were freely varied in order to match the observed temperature profiles in wells. Several such calculations were carried out; in the following, we will only describe the final case.

Formation properties utilized for the Mountain Home natural-state model are given in Table 1. Distribution of the formation properties within the model grid is shown in Figures 4a to 4q. Rock types assigned to individual grid blocks (Figures 4a-q) are based on lithological logs from wells MH-1, MH-2, and Bostic1. The average vertical permeability at Mountain Home appears to be

rather low. More specifically, a low vertical permeability is required for matching the mostly conductive temperature profiles recorded in the area wells. As mentioned previously, the assumed horizontal permeabilities are essentially arbitrary, and are unconstrained at the present time.

In addition to formation properties given in table 1, it is necessary to specify capillary pressure and relative permeabilities. The capillary pressure is assumed to be negligible. Straight-line relative permeability curves with a liquid (gas) residual saturation of 0.2 (0.0) are used. Since two-phase flow is unlikely in the "natural state" at Mountain Home, the capillary pressure and relative permeability have no effect on the computed natural-state.

Table 1: Formation properties.

Formation Name	Intrinsic rock density (kg/m^3)	Rock grain specific heat (J/kg-^oC)	Global Thermal Conductivity (W/m-^oC)	Porosity	Permeability in x-direction (mdarcy)*	Permeability in y-direction (mdarcy)*	Permeability in z-direction (mdarcy)*
1.Sediments/basalt	2800	1000	1.5	0.100	5	5	0.1
2.Basalt upper	2800	1000	1.5	0.025	5	5	1
3.Basalt Lower	2800	1000	1.5	0.025	5	5	1
4.Rhyolite/basalt	2800	1000	1.5	0.025	1	1	0.1

*It is assumed here that 1 millidarcy is exactly equal to 10^{-15} m^2

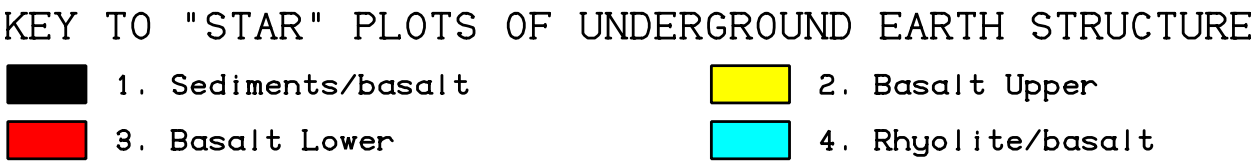

Figure 4a: Key to earth structure; see table 1 for formation properties.

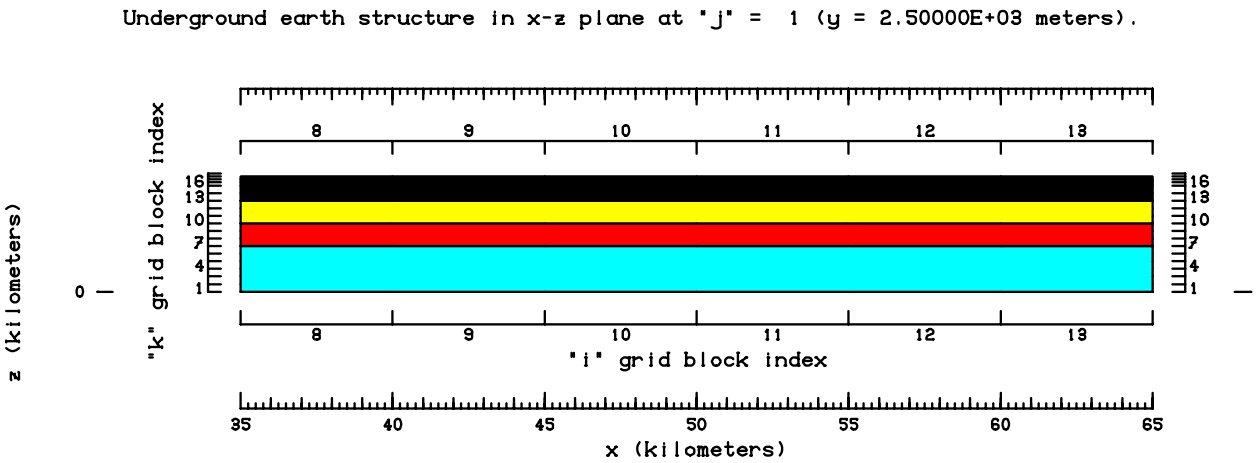

Figure 4b: Earth structure in x-z plane (j=1).Note that only a part of the grid (i=8 to 13) is shown.

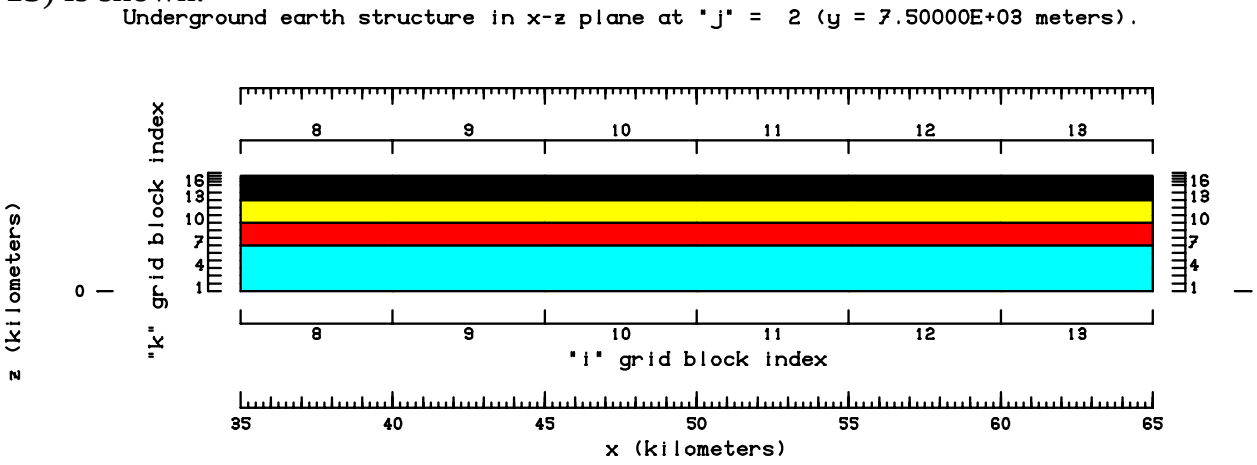

Figure 4c: Earth structure in x-z plane (j=2). Note that only a part of the grid (i=8 to 13) is shown.

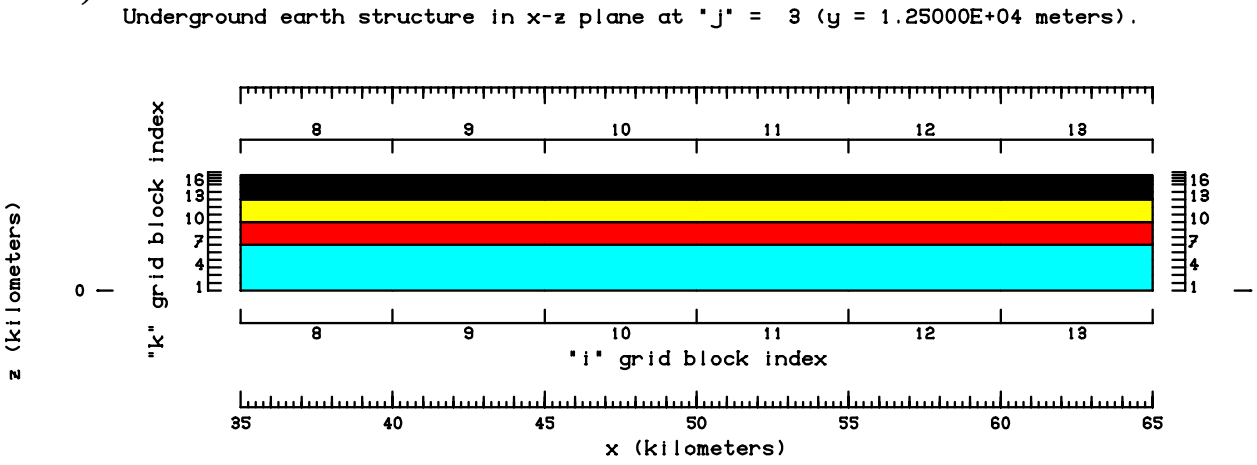

Figure 4d: Earth structure in x-z plane (j=3). Note that only a part of the grid (i=8 to 13) is shown.

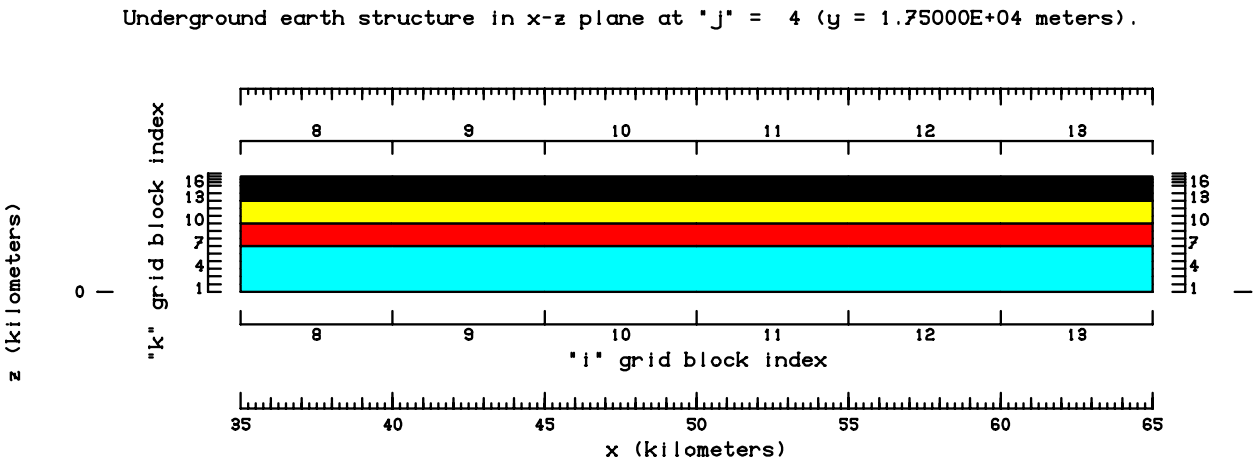

Figure 4e: Earth structure in x-z plane (j=4). Note that only a part of the grid (i=8 to 13) is shown.

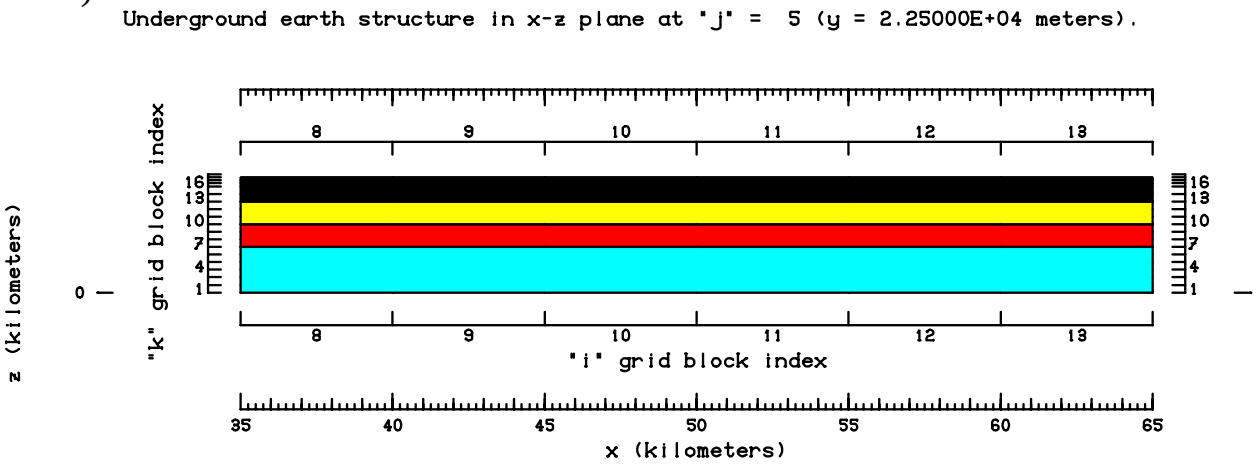

Figure 4f: Earth structure in x-z plane (j=5). Note that only a part of the grid (i=8 to 13) is shown.

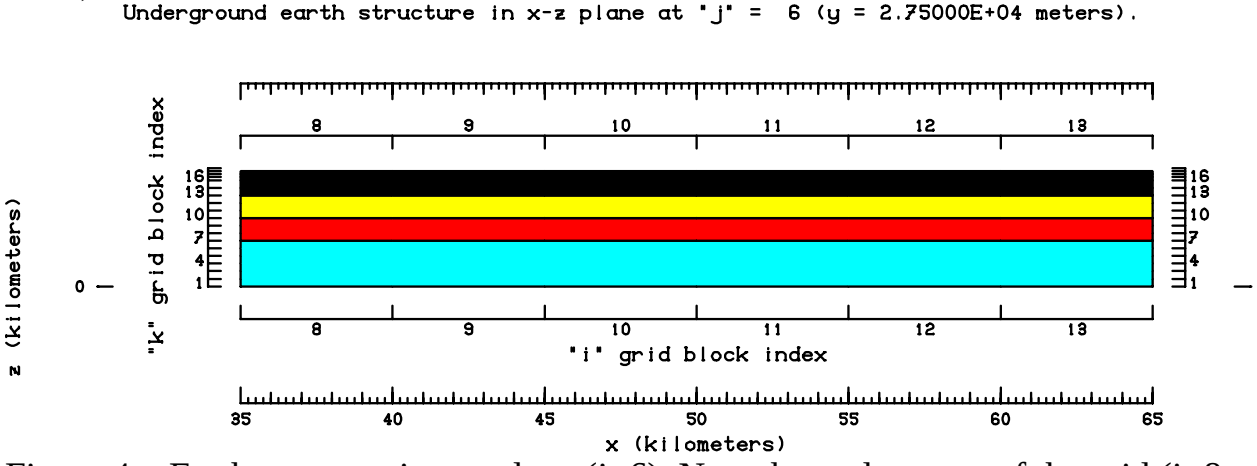

Figure 4g: Earth structure in x-z plane (j=6). Note that only a part of the grid (i=8 to 13) is shown.

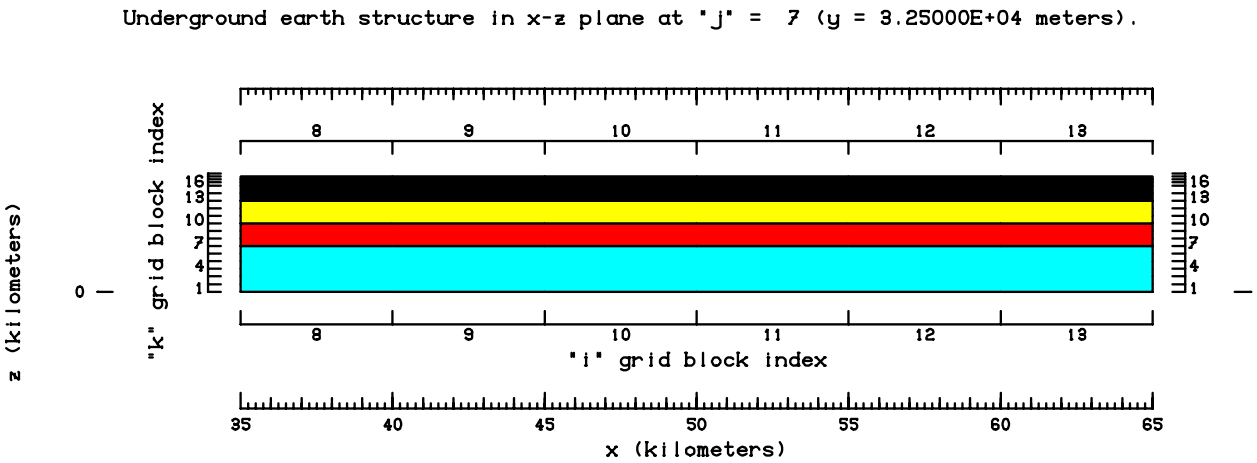

Figure 4h: Earth structure in x-z plane (j=7). Note that only a part of the grid (i=8 to 13) is shown.

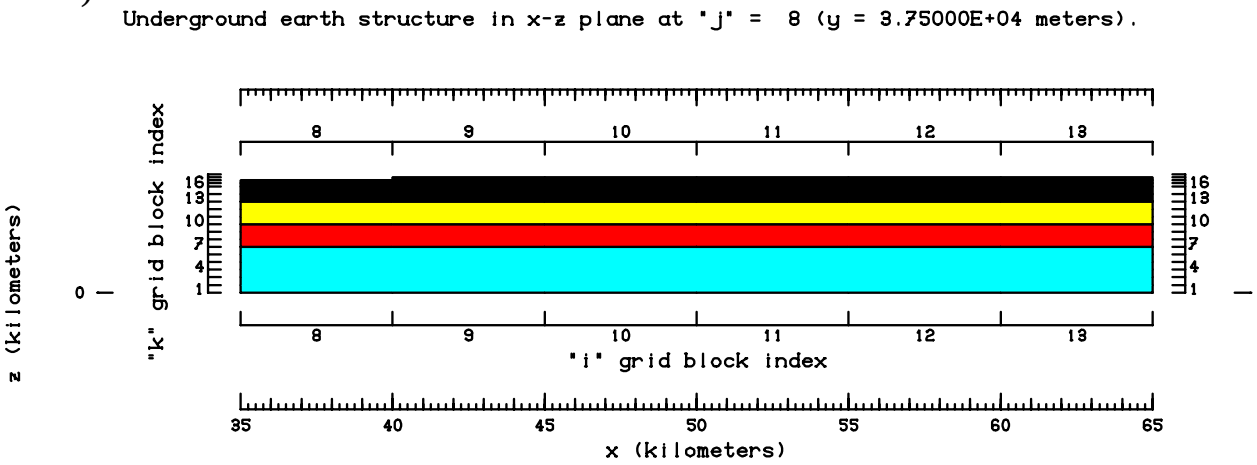

Figure 4i: Earth structure in x-z plane (j=8). Note that only a part of the grid (i=8 to 13) is shown.

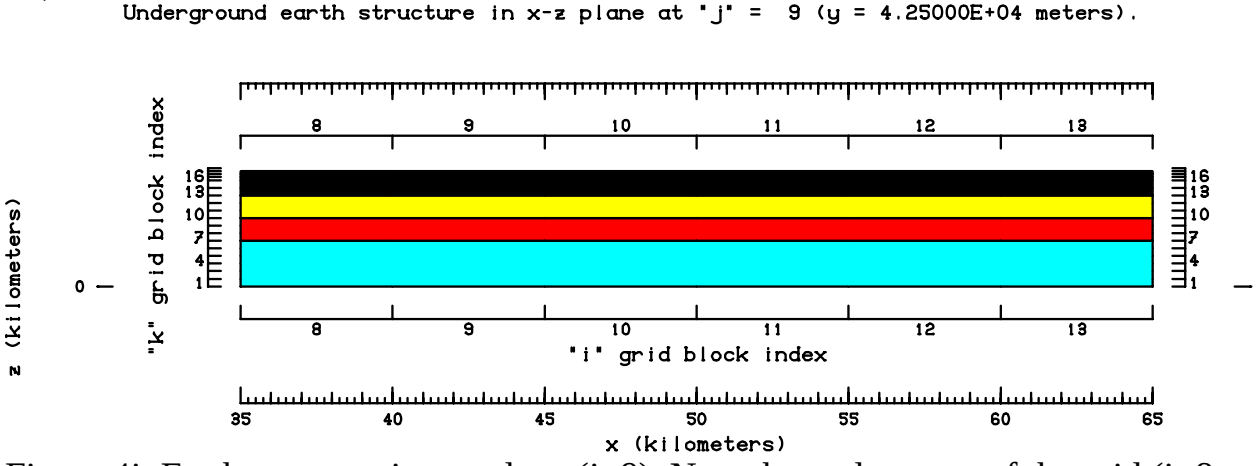

Figure 4j: Earth structure in x-z plane (j=9). Note that only a part of the grid (i=8 to 13) is shown.

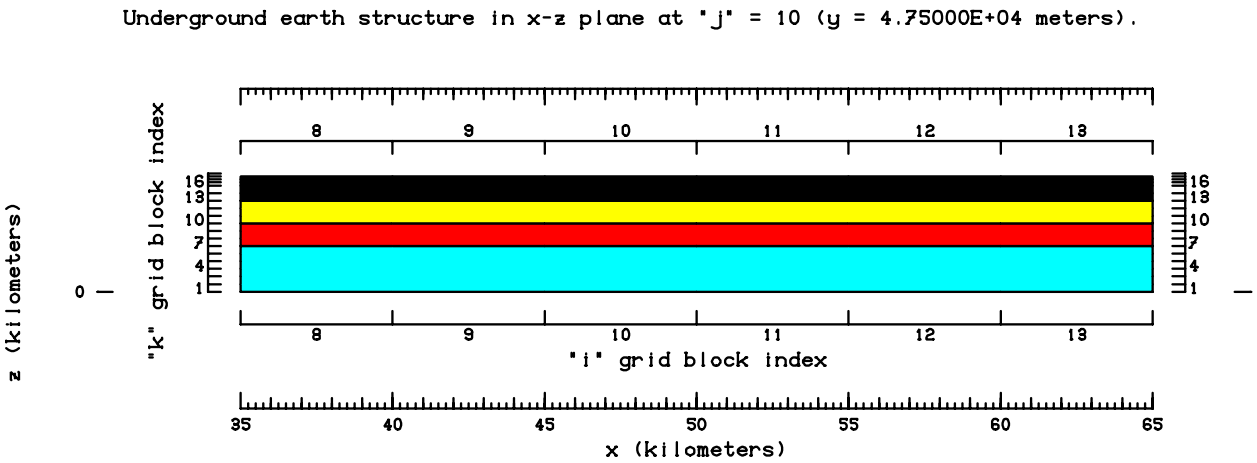

Figure 4k: Earth structure in x-z plane (j=10). Note that only a part of the grid (i=8 to 13) is shown.

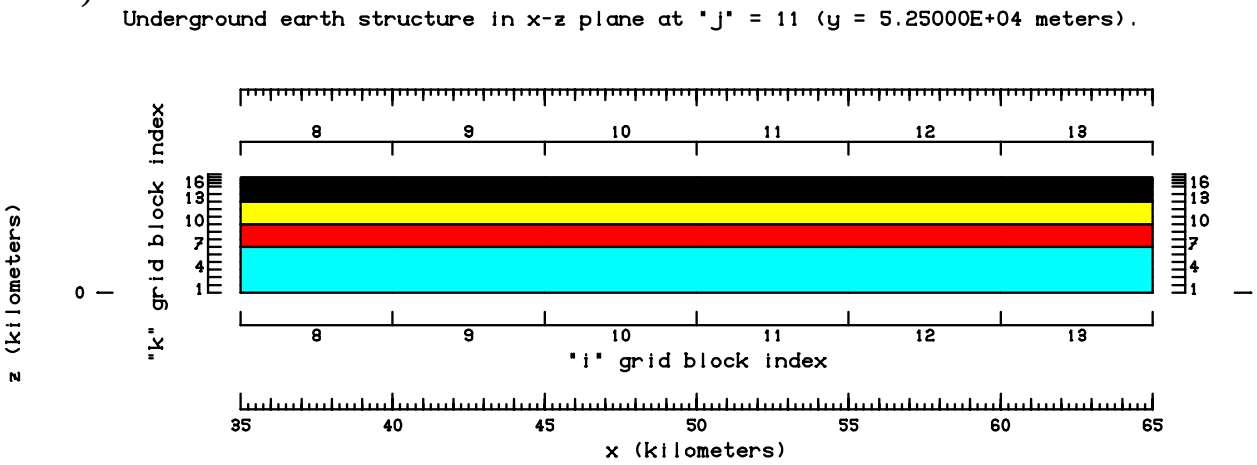

Figure 4l: Earth structure in x-z plane (j=11). Note that only a part of the grid (i=8 to 13) is shown.

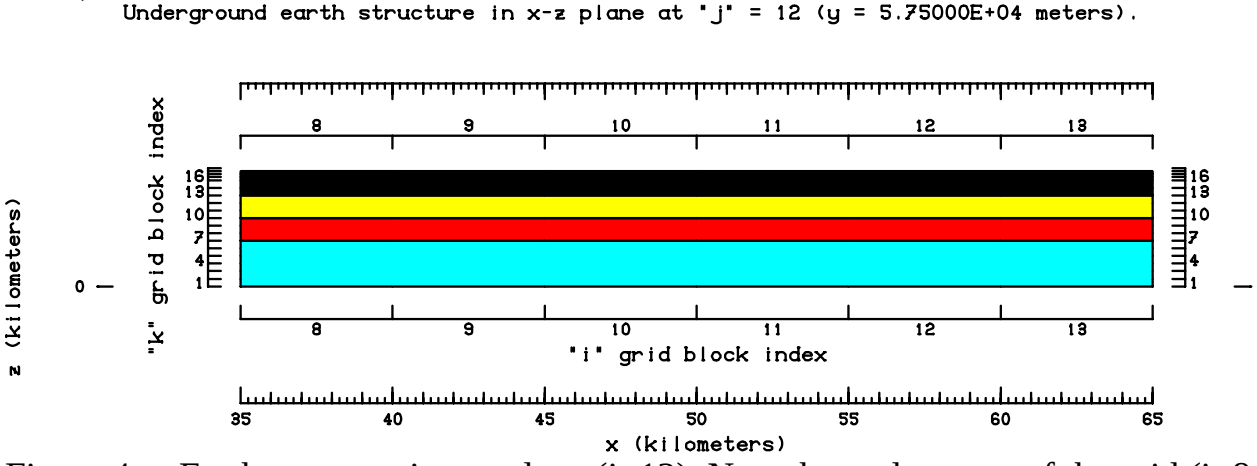

Figure 4m: Earth structure in x-z plane (j=12). Note that only a part of the grid (i=8 to 13) is shown.

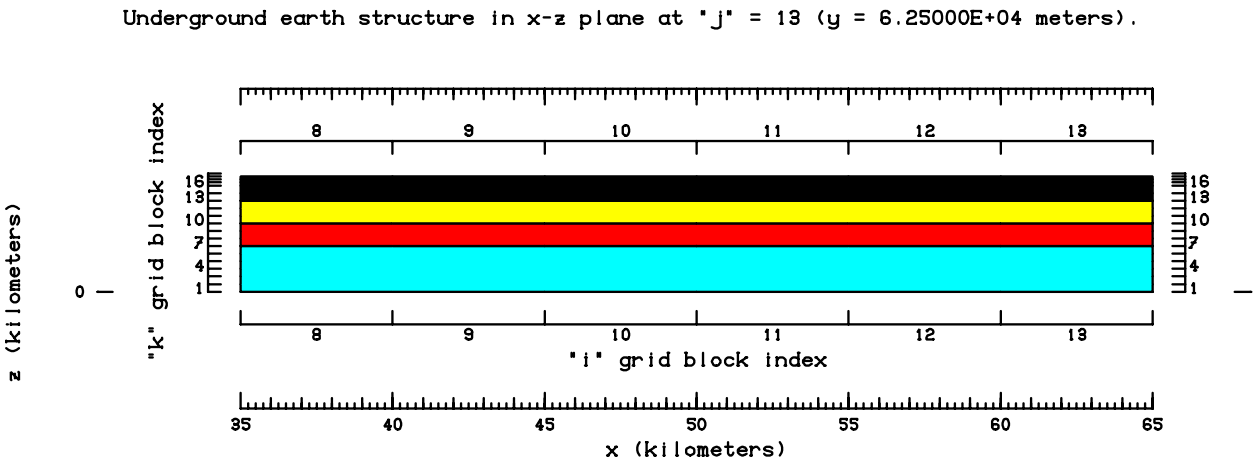

Figure 4n: Earth structure in x-z plane (j=13). Note that only a part of the grid (i=8 to 13) is shown.

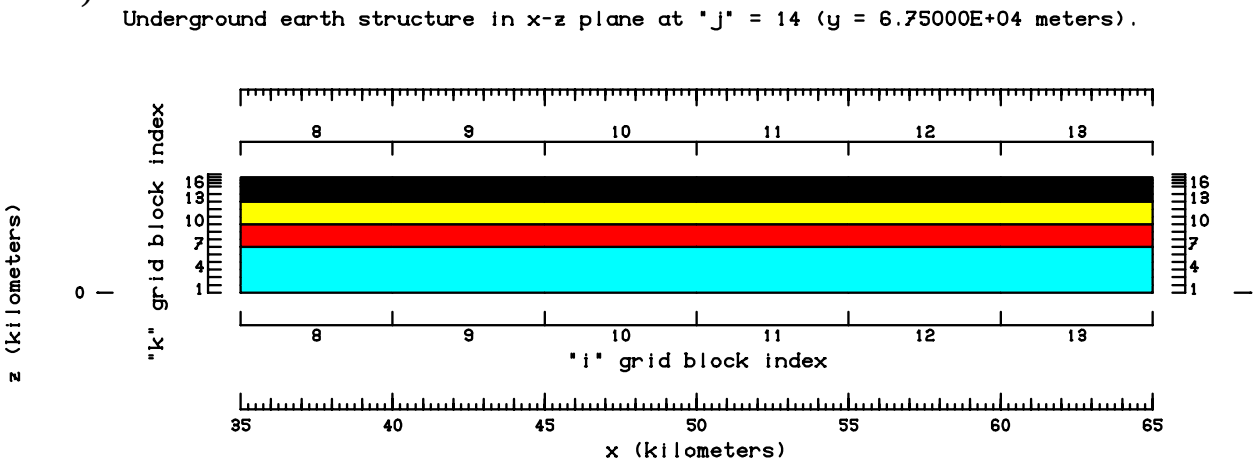

Figure 4o: Earth structure in x-z plane (j=14). Note that only a part of the grid (i=8 to 13) is shown.

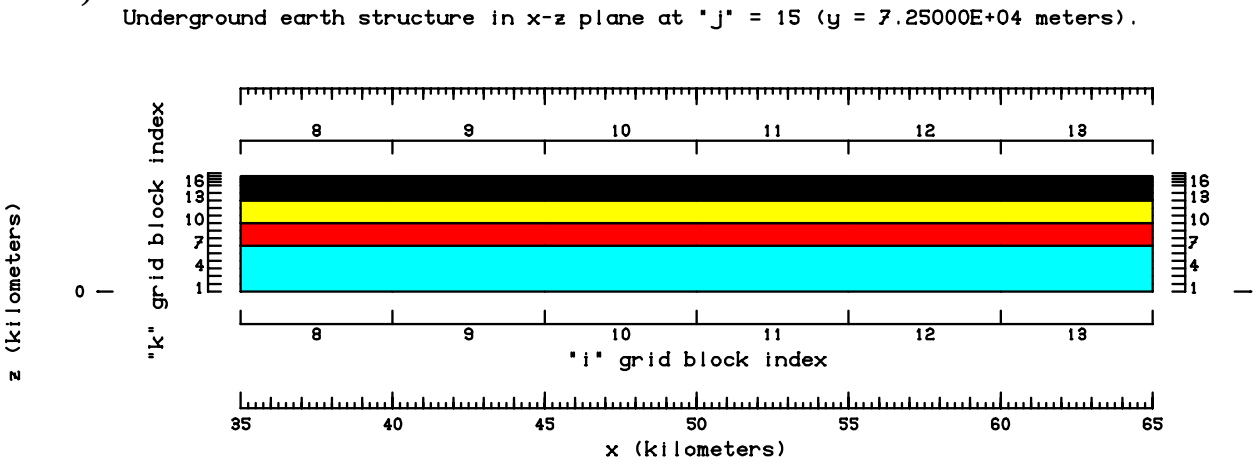

Figure 4p: Earth structure in x-z plane (j=15). Note that only a part of the grid (i=8 to 13) is shown.

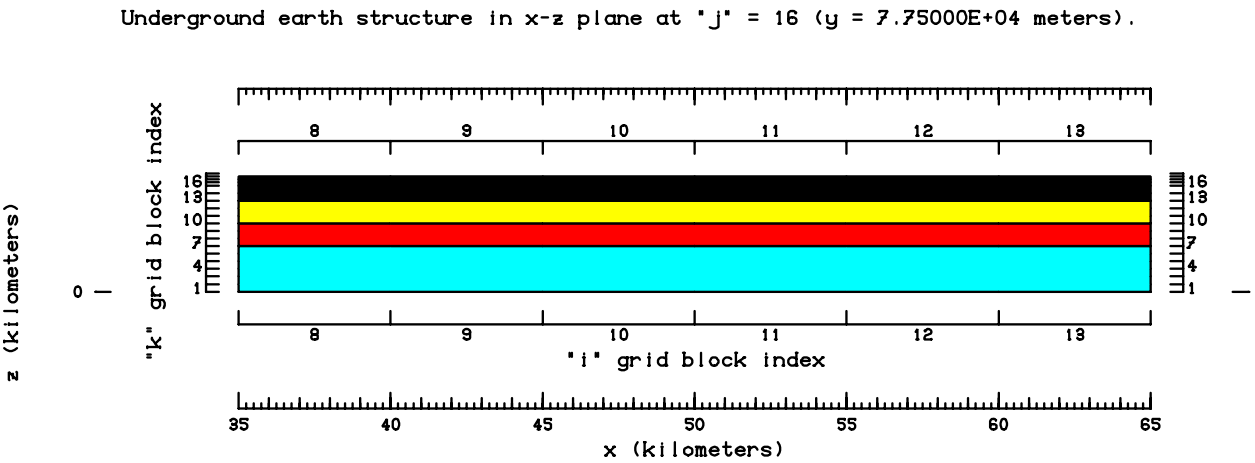

Figure 4q: Earth structure in x-z plane (j=16). Note that only a part of the grid (i=8 to 13) is shown.

Along the top boundary, the water table (i.e. 1 bar surface) is assumed to be at an elevation given by:

$$z_w = 0.10(z - 750) + 750 = 0.10z + 675 \qquad (1)$$

where z_w denotes the water table elevation (mASL) and z is the local ground surface elevation. The ground surface temperature and shallow subsurface temperature gradient are assumed to be 10 ^{o}C and 85 ^{o}C/km, respectively. If the water table given by Eq. (1) falls below the mid-point of a grid block, the grid block is flagged as void. Use of Eq. (1) renders many grid blocks in layers k=17 and k=18 void. Sources and sinks are imposed in all the top-most grid blocks in each vertical column (i, j; i=1, …, 22, and j=1, …, 16) to maintain the pressures and temperatures consistent with Eq. (1), and the assumed surface temperature and shallow subsurface temperature gradient.

Along the bottom boundary, a non-uniform conductive heat flux is imposed along the entire surface (see Figure 5). All the vertical faces of the grid are assumed to be impermeable and insulated. The reservoir fluid is treated as pure water.

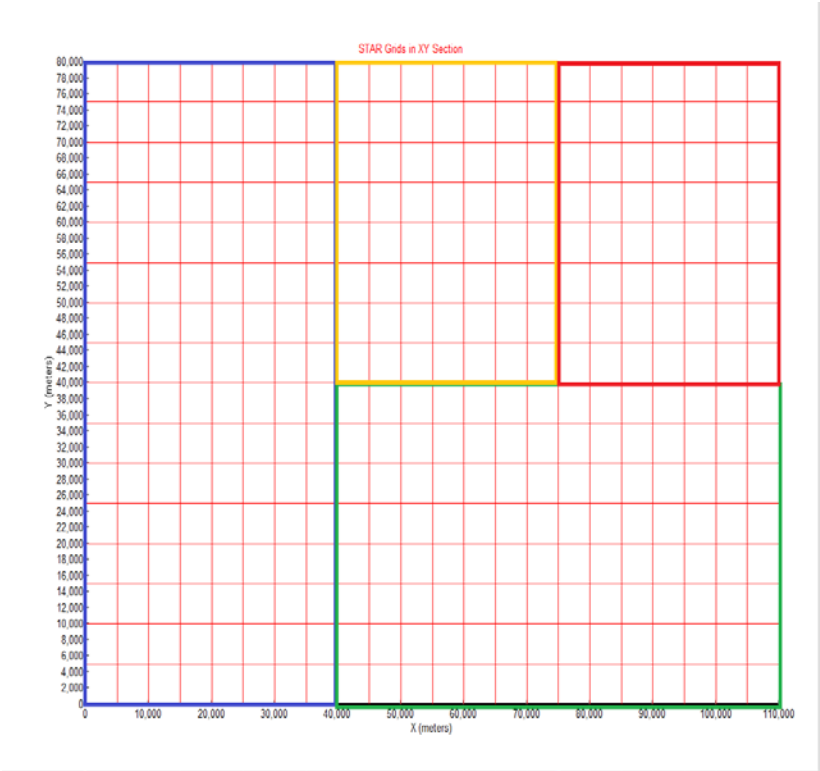

Figure 5: Heat flux distribution along the bottom boundary. Area enclosed by 1. blue outline, heat flux = 60 mW/m^2, 2. green outline, heat flux = 75 mW/m^2, 3. yellow outline, heat flux = 100 mW/m^2, and 4. Red outline, heat flux = 110 mW/m^2.

IV. Computation of Quasi-Steady Natural State

Starting from an essentially arbitrary cold state, the computation was marched forward in time for about 625,000 years. The maximum time step used was 25 years. The change in total thermal energy and fluid mass in the computational grid is displayed in Figures 6 and 7. For most of the computational period, the thermal energy continues to increase and the fluid mass declines. Initially the change is rapid; it moderates over time. After about 500,000, the change is quite small over a time scale of 50 to 100 years. The computed temperature values at cycle 15,000 (about 625,000 years) were compared with the available data.

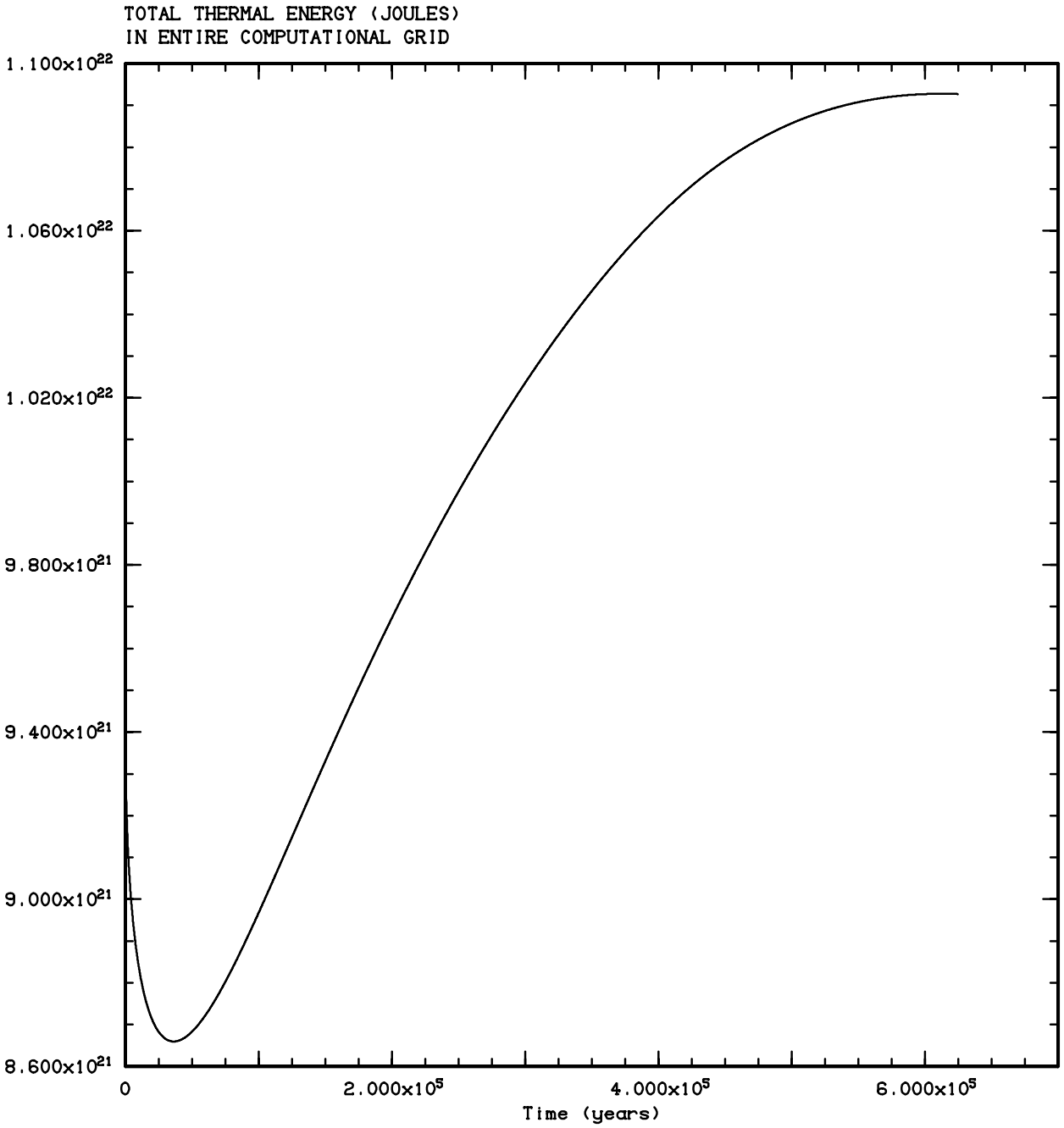

Figure 6: Computed total thermal energy in the computational grid.

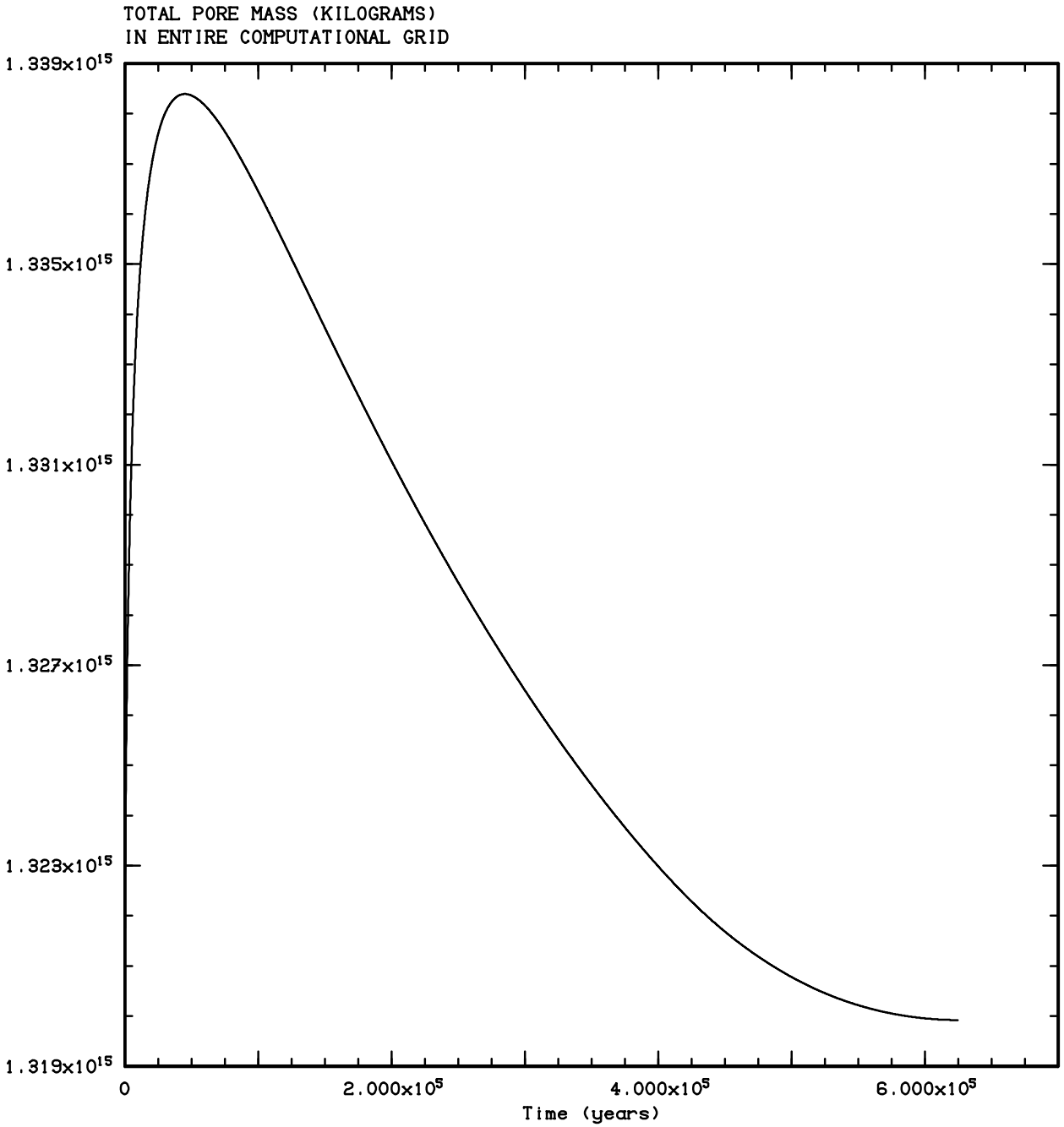

Figure 7: Computed total fluid mass in the computational grid.

The measured temperatures in Mountain Home wells are compared with calculated results from the model in Figures 8a-m. For most of the wells, it is not known if the available temperature data represent stable formation temperatures. The only available temperature survey for well Lawrence D No.1 was obtained after a shut-in time of 8 hours, and the measured temperatures are in all likelihood much lower than the undisturbed formation temperatures. Well Anschutz No. 1 is quite close to well Lawrence D No. 1; measured temperatures (shut-in time ~ 66 hours)

in the Anschutz well are considerably higher than those recorded in the Lawrence well. No information on shut-in time is available regarding the temperature surveys in other area wells. Given the current data limitations, the agreement between the measured and computed temperature values is considered satisfactory.

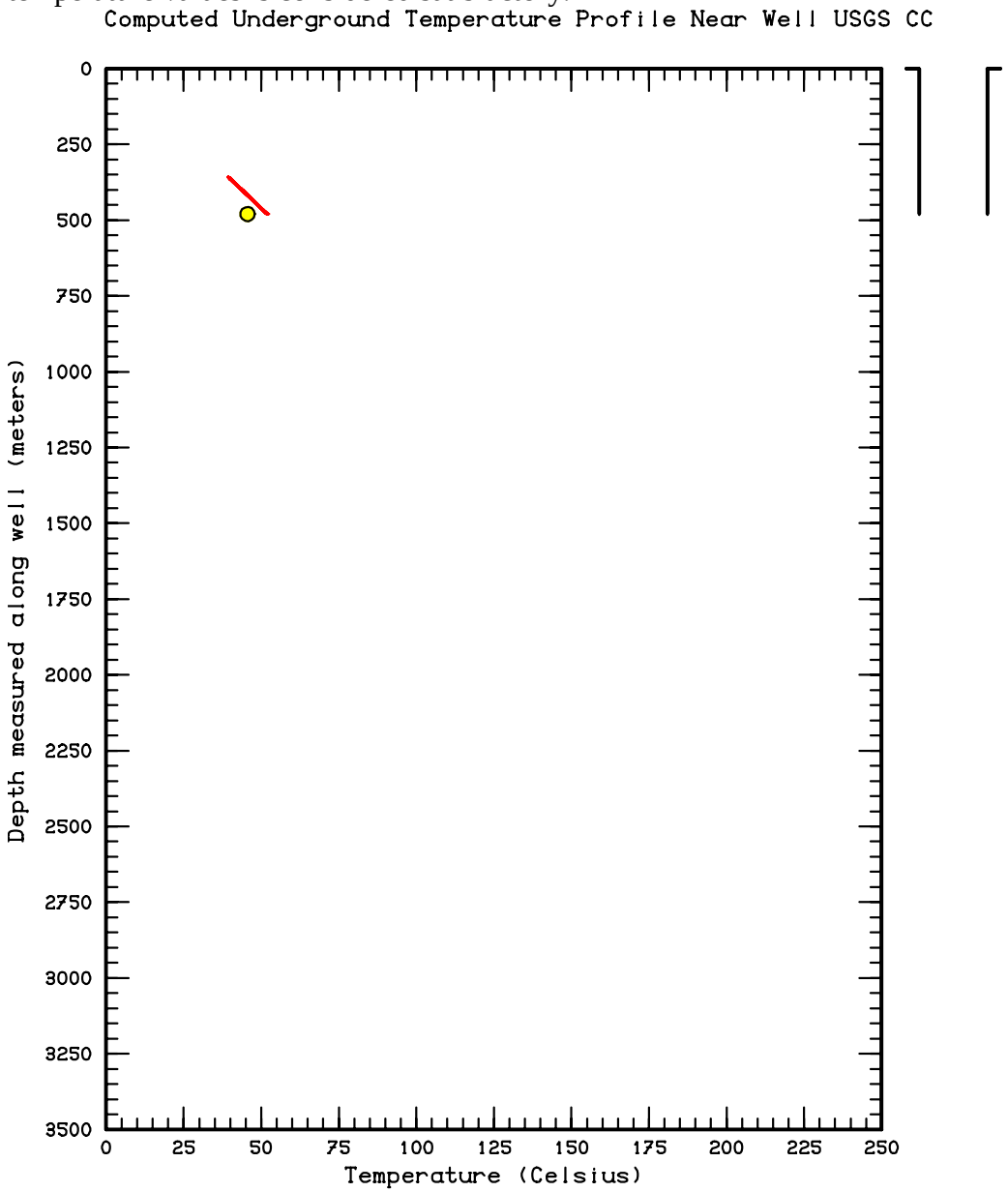

Figure 8a: Comparison between computed solid red line) and measured temperature profiles (yellow circle) for well USGS CC.

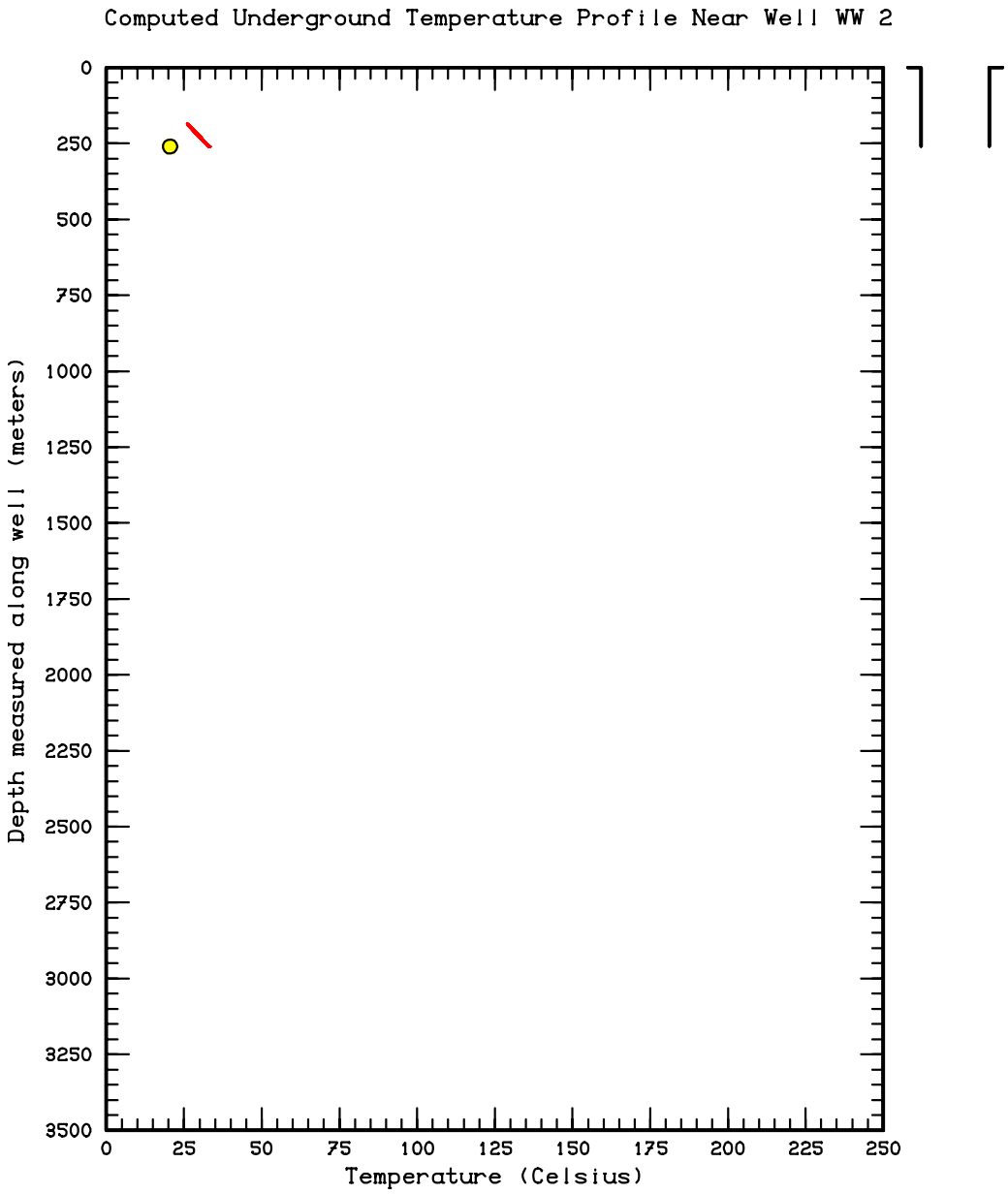

Figure 8b: Comparison between computed (solid red line) and measured temperature profiles (yellow circle) for well WW2.

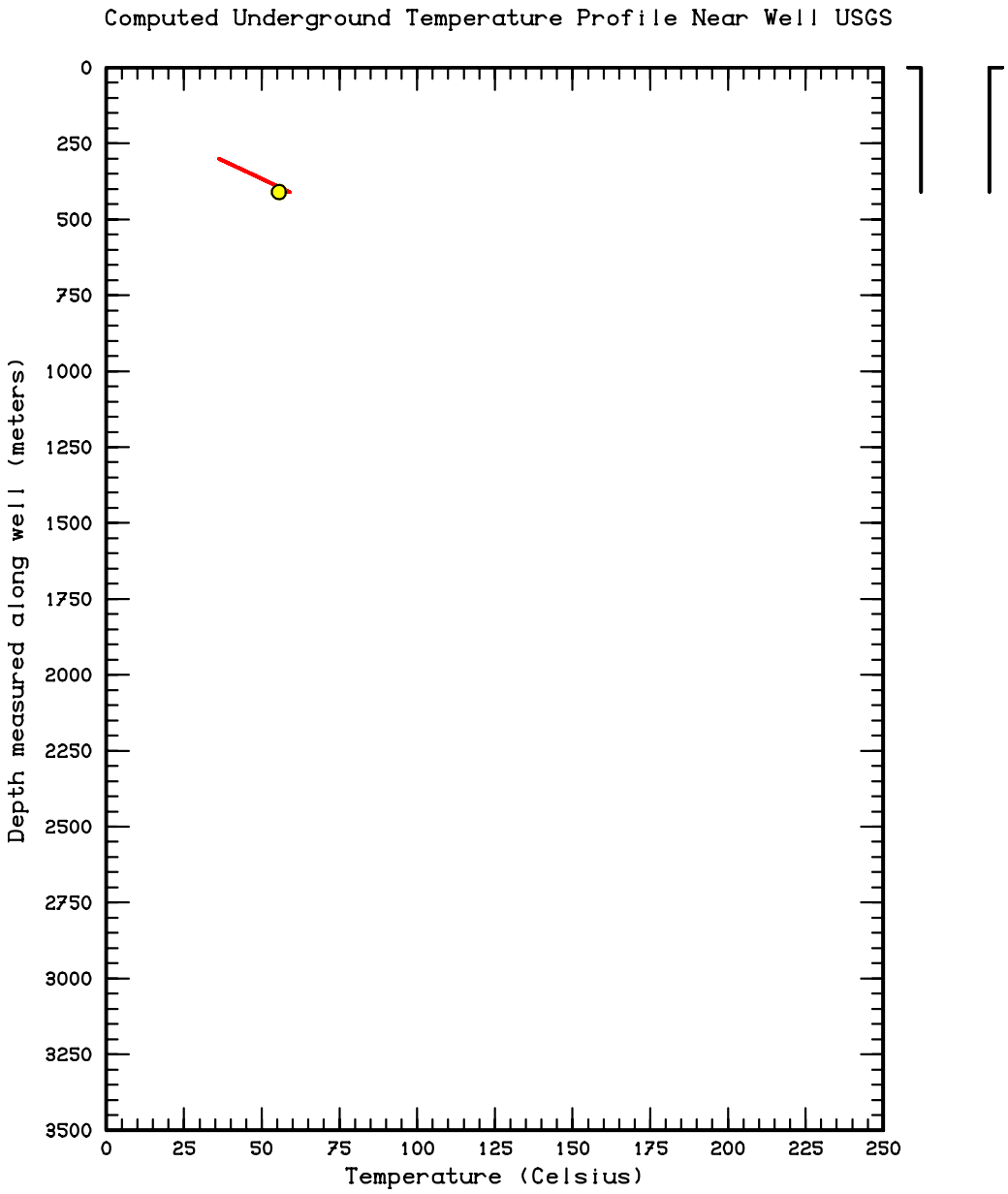

Figure 8c: Comparison between computed (solid red line) and measured temperature profiles (yellow circle) for well USGS.

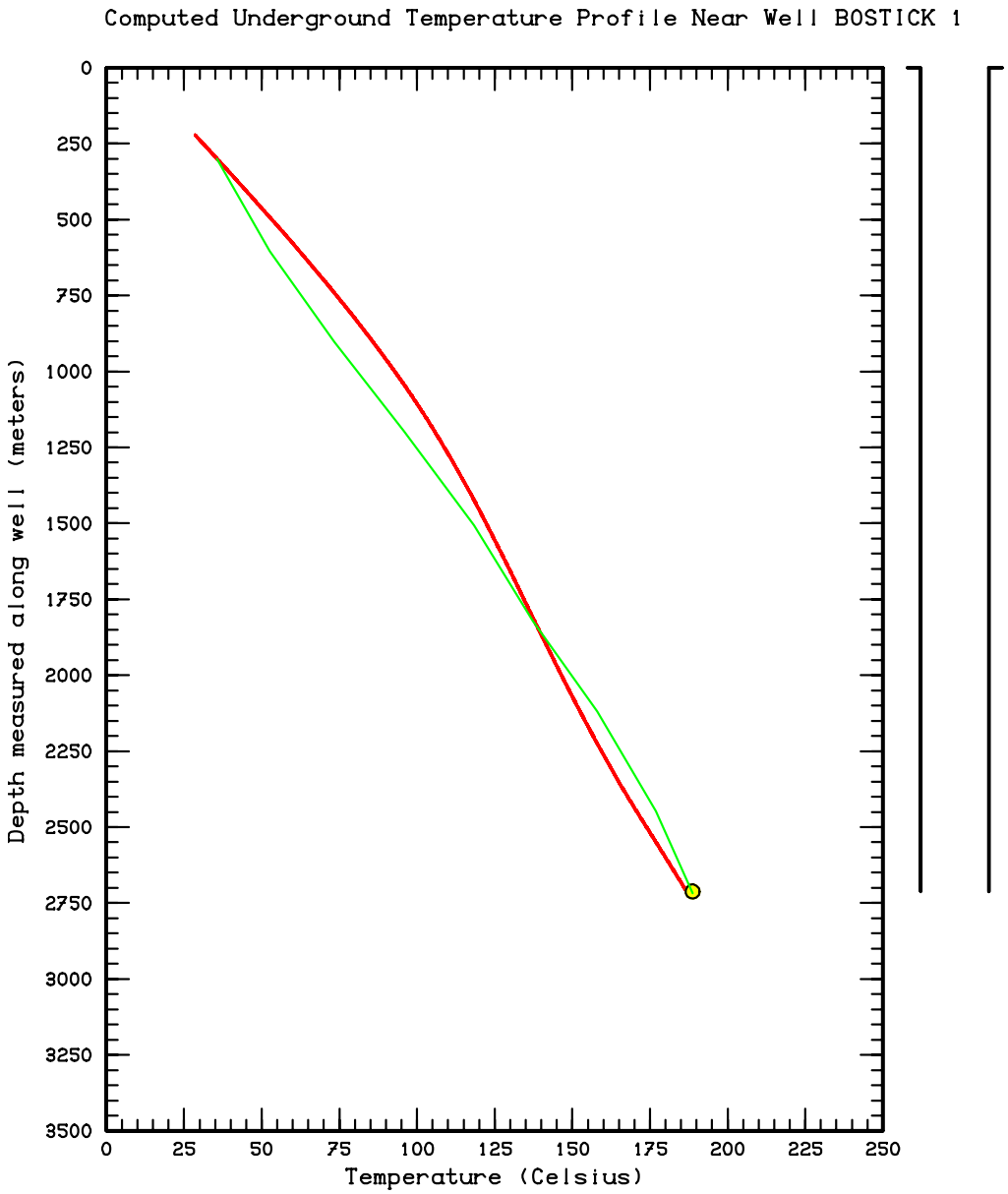

Figure 8d: Comparison between computed (solid red line) and measured temperature profiles (solid green line and yellow circle) for well Bostic1. No information is available concerning the shut-in time at which the temperature survey was taken.

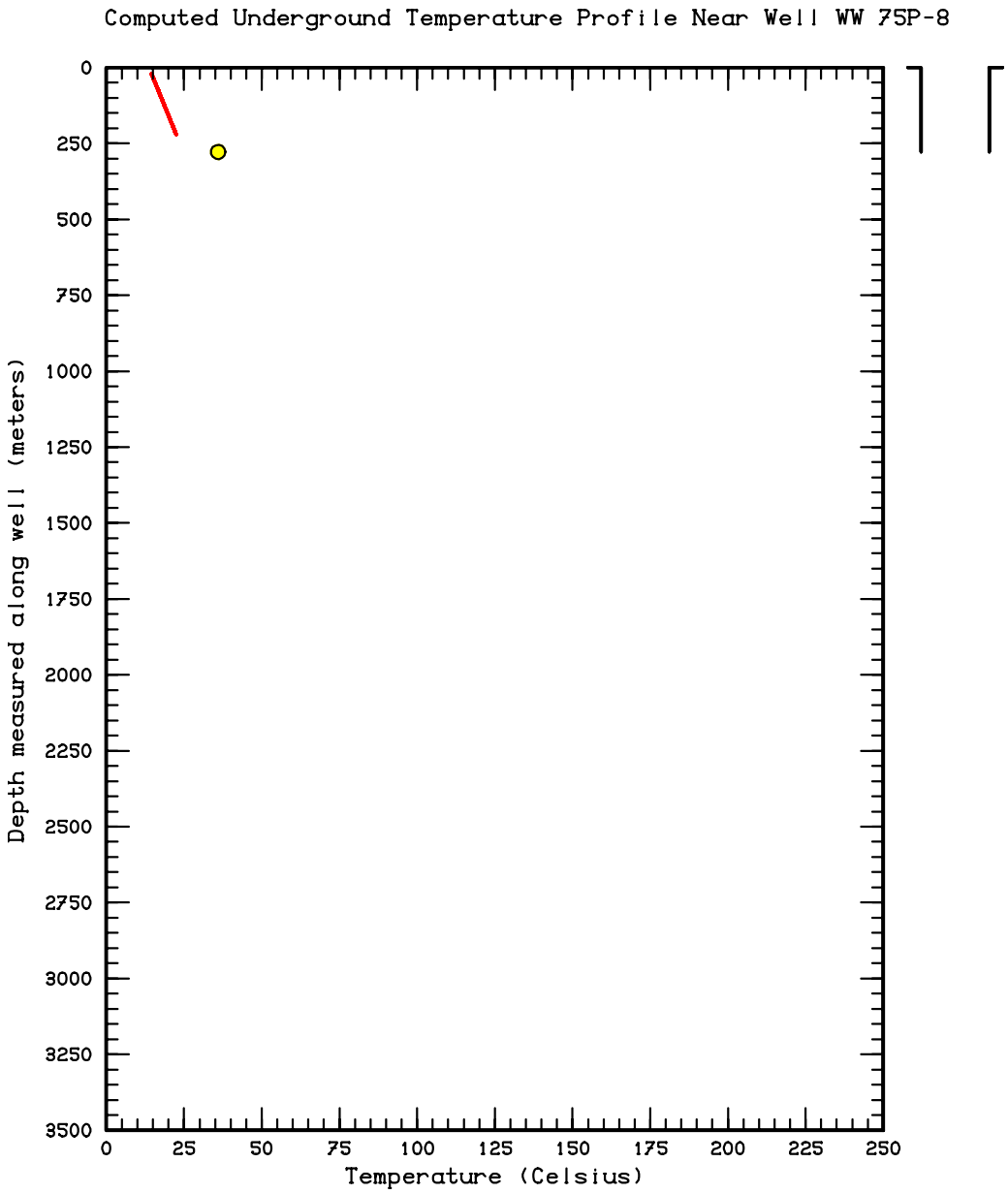

Figure 8e: Comparison between computed (solid red line) and measured temperature profiles (yellow circle) for well WW 75P-8.

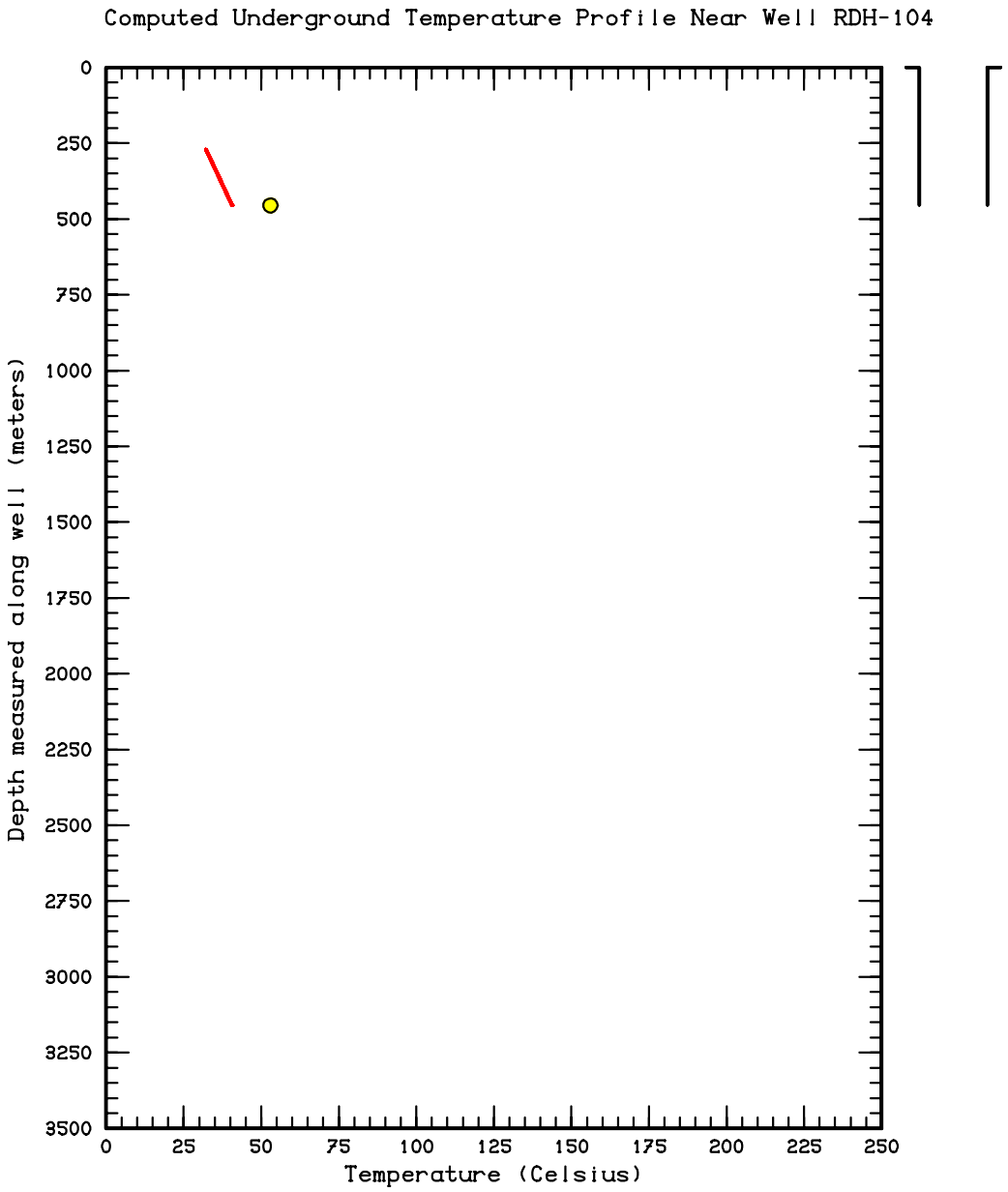

Figure 8f: Comparison between computed (solid red line) and measured temperature profiles (yellow circle) for well RDH-104.

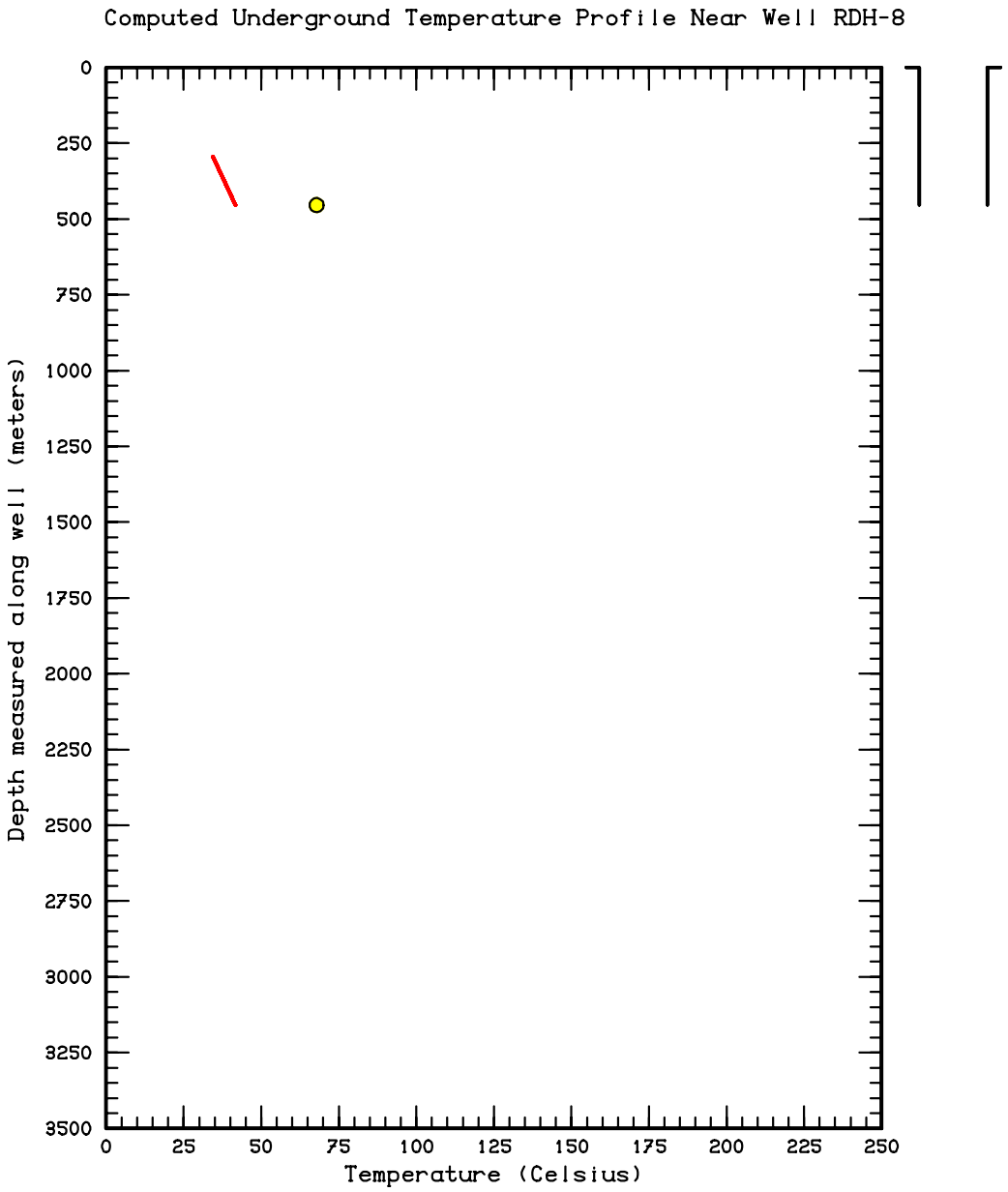

Figure 8g: Comparison between computed (solid red line) and measured temperature profiles (yellow circle) for well RDH-8.

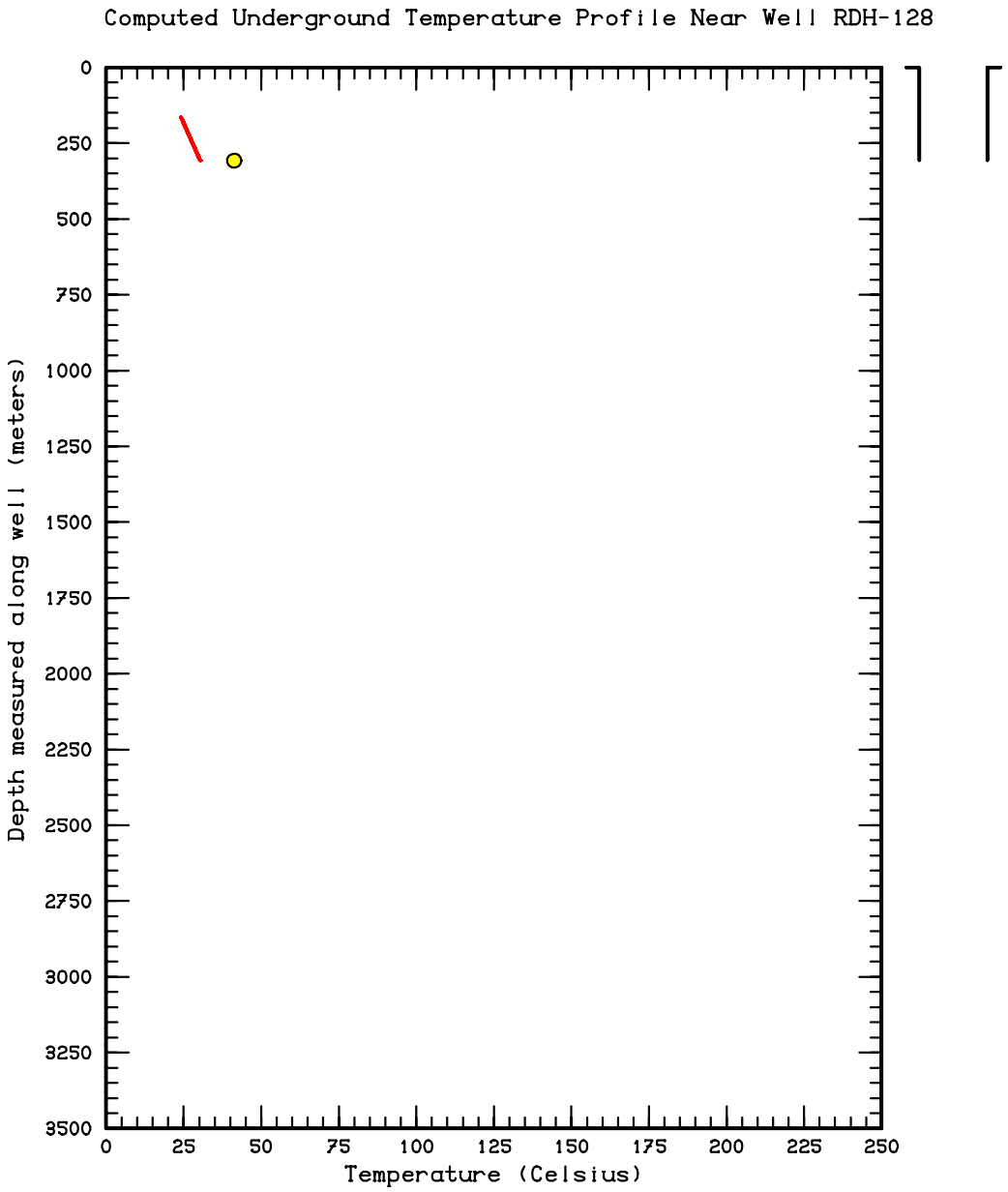

Figure 8h: Comparison between computed (solid red line) and measured temperature profiles (yellow circle) for well RDH-128.

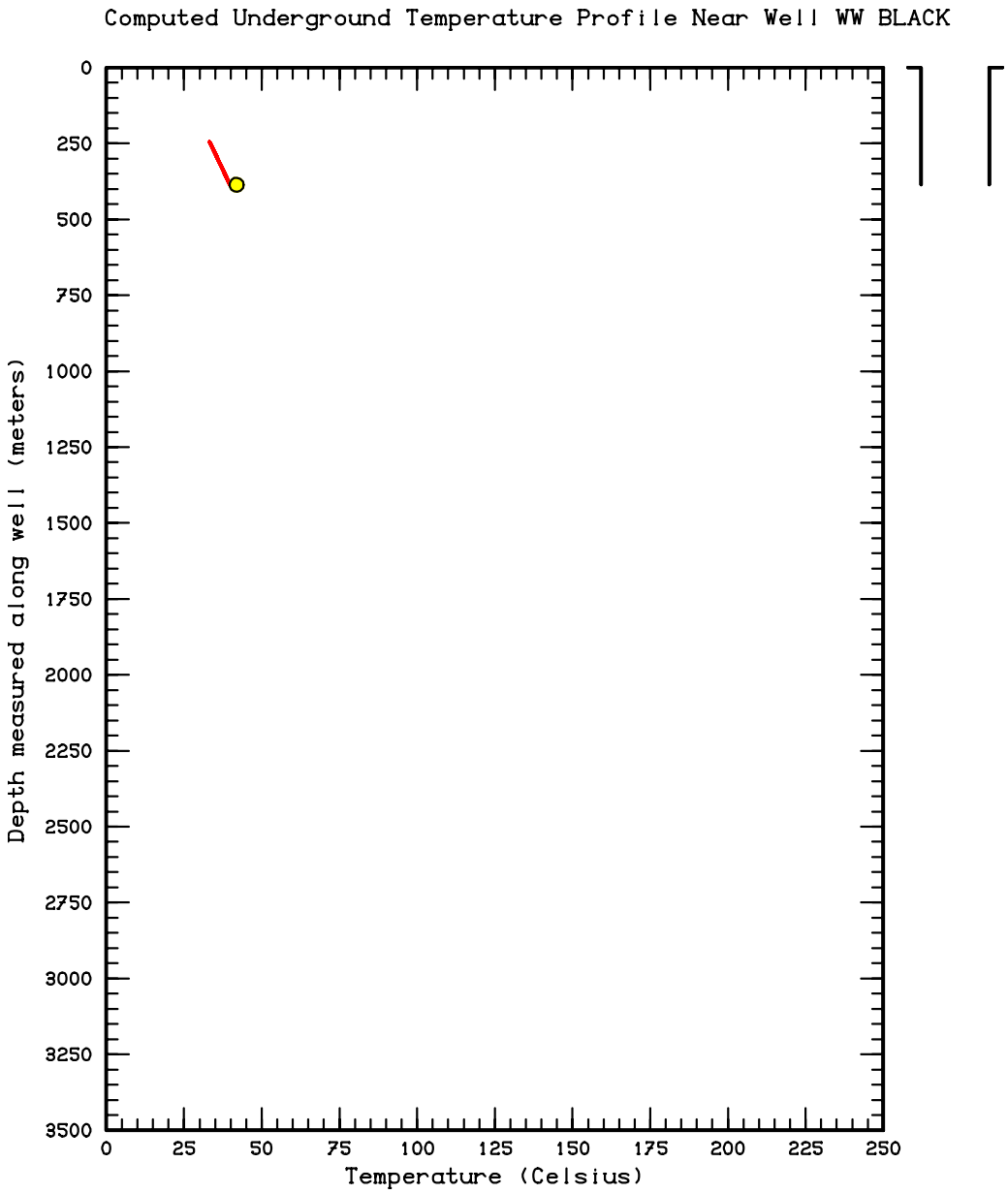

Figure 8i: Comparison between computed (solid red line) and measured temperature profiles (yellow circle) for well WW Black.

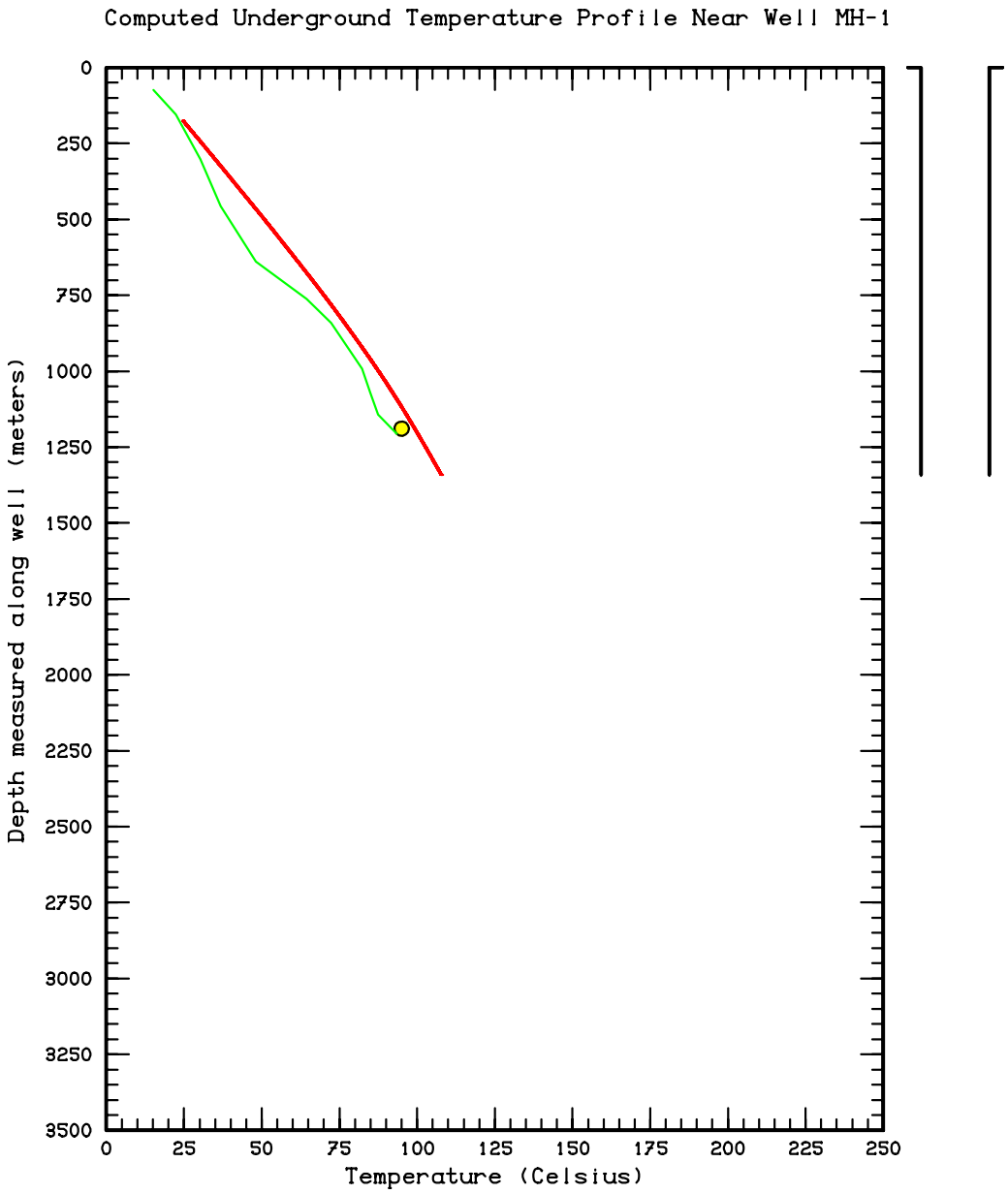

Figure 8j: Comparison between computed (solid red line) and measured temperature profiles (solid green line and yellow circle) for well MH-1. No information is available concerning the shut-in time at which the temperature survey was taken.

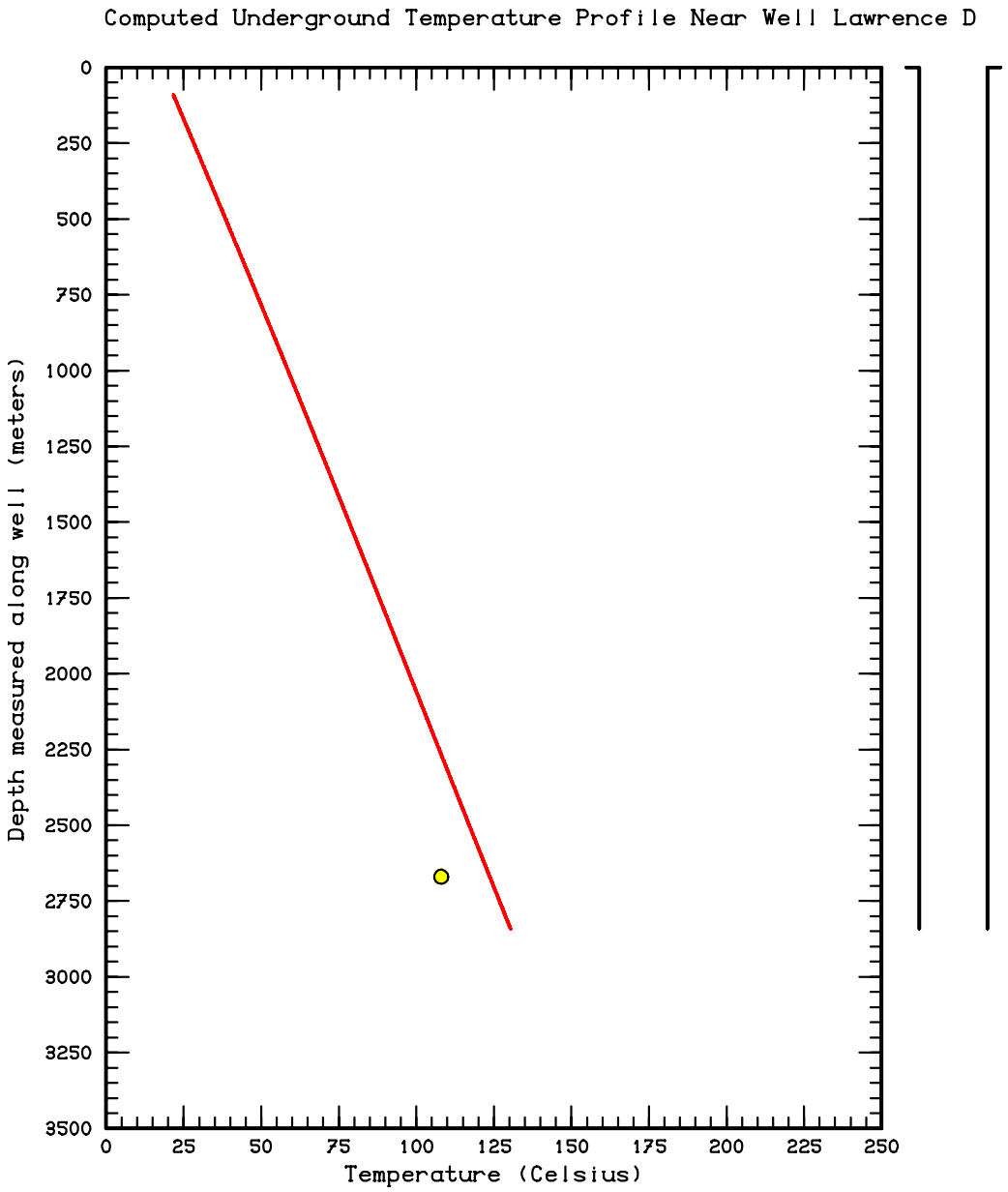

Figure 8k: Comparison between computed (solid red line) and measured temperature profiles (yellow circle) for well Lawrence D No. 1. The measured temperature was recorded after the well had been shut-in for only about 8 hours.

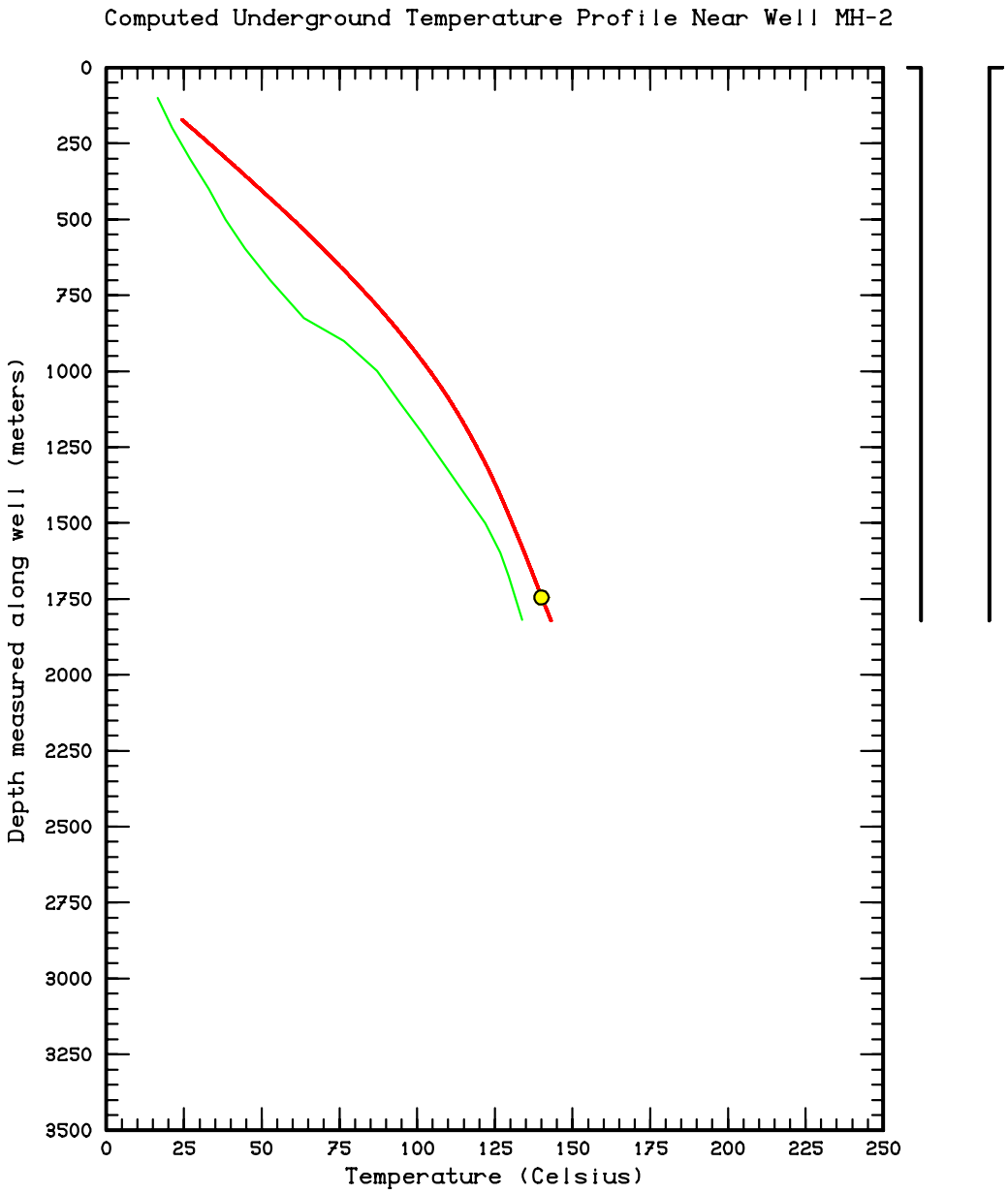

Figure 8l: Comparison between computed (solid red line) and measured temperature profiles (solid green line) for well MH-2. No information is available concerning the shut-in time at which the temperature survey was taken. The yellow circle is the measured flowing temperature at this depth. Since the measured flowing temperature is higher than the recorded shut-in temperature (solid green line), it is almost certain that the shut-in survey does not represent the stable formation temperatures.

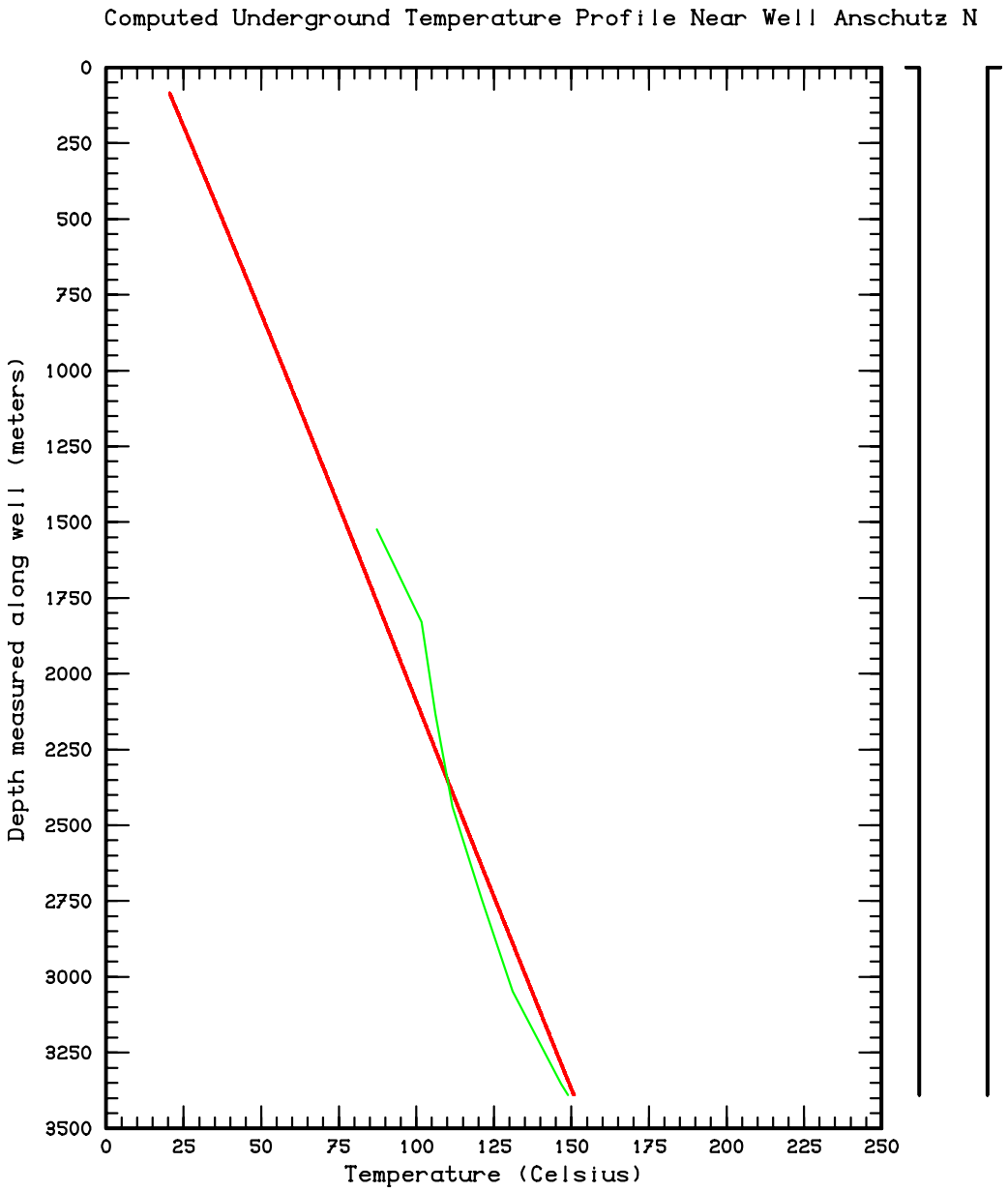

Figure 8m: Comparison between computed (solid red line) and measured temperature profiles (solid green line) for well Anschutz No. 1. The temperature survey was taken after the well had been shut-in for about 66 hours.

V. Computed Temperature Distribution and Fluid Flow

Computed temperatures and fluid flux vectors in horizontal x-y planes are exhibited in Figures 9a to 9r. The highest ground at Mountain Home (see Figure 2) is to the northeast and southwest; these areas are the recharge areas (see Figures 9o to 9q; layers k=15 to 17); the flow is generally to the northeast from southwest and southwest from northeast. The latter flow pattern, especially from that from southwest to northeast, persists at depth. Fluid flow pattern and temperature isotherms are rather complicated in the northeast part of the computational grid. The top of the grid lies in layers k=16, k=17 and k=18 (Figures 9p, 9q and 9 r); temperatures and pressures in the topmost zone in each i-j column are kept fixed and vary with the surface topography.

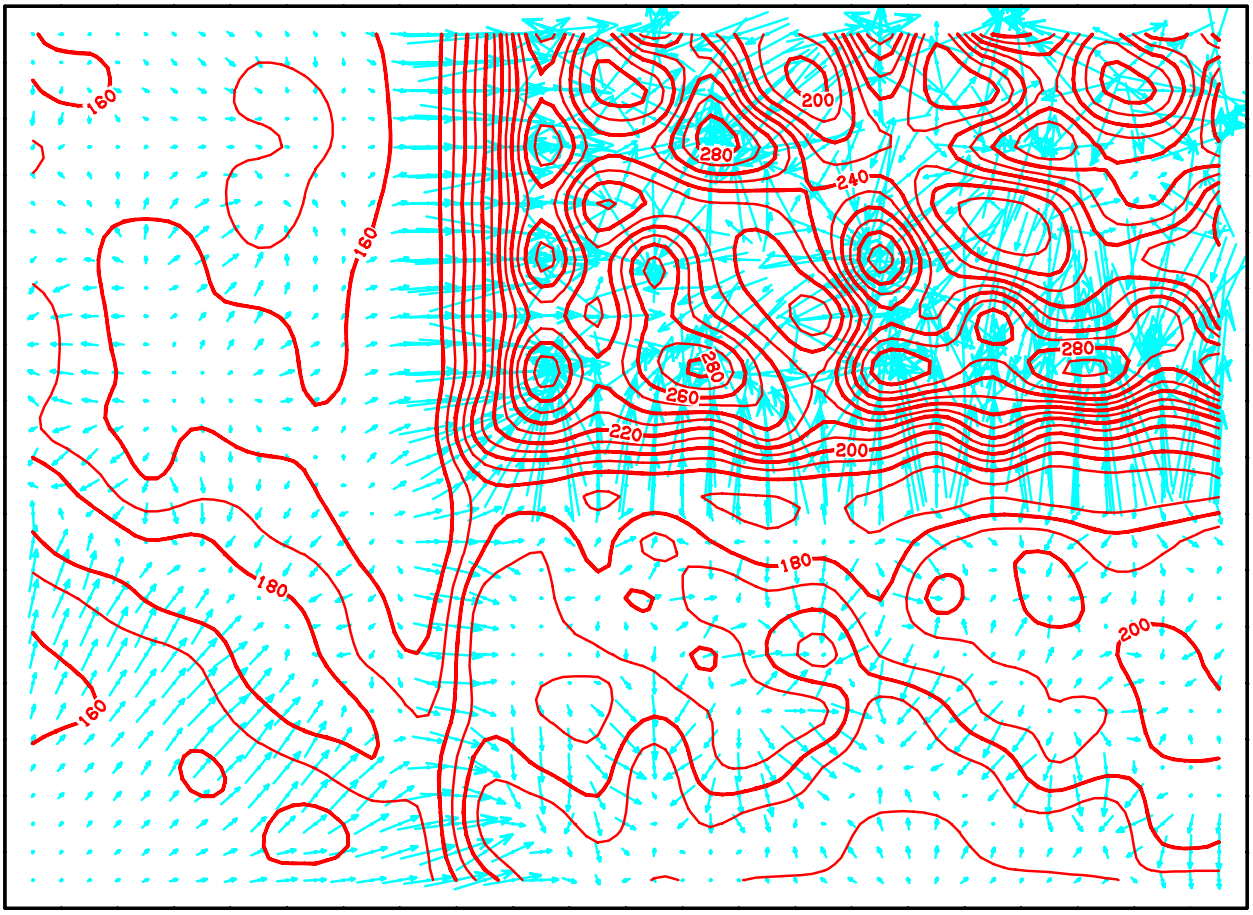

Figure 9a: Isotherms (red lines) and flow vectors (blue) in the vertical x-y plane k=1.

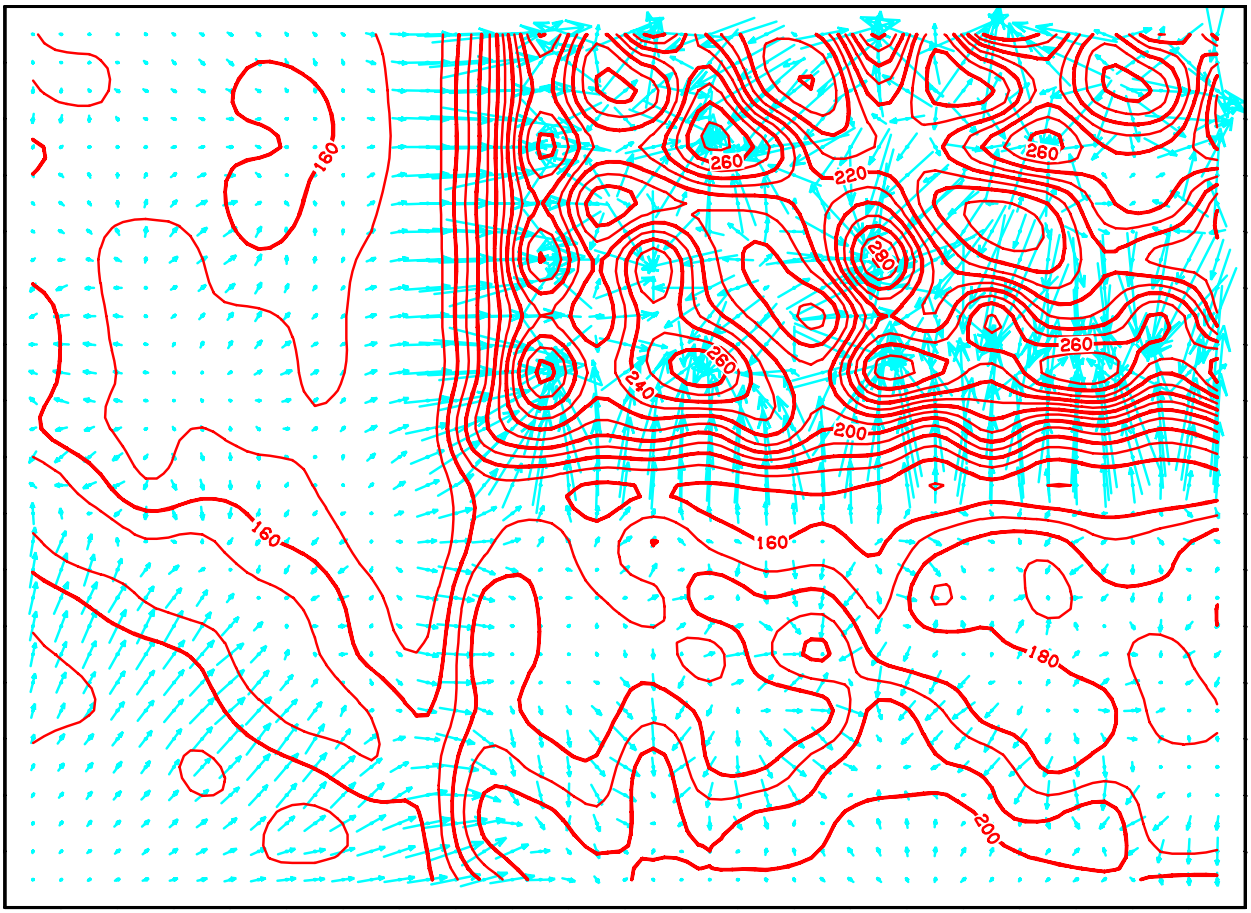

Figure 9b: Isotherms (red lines) and flow vectors (blue) in the vertical x-y plane k=2.

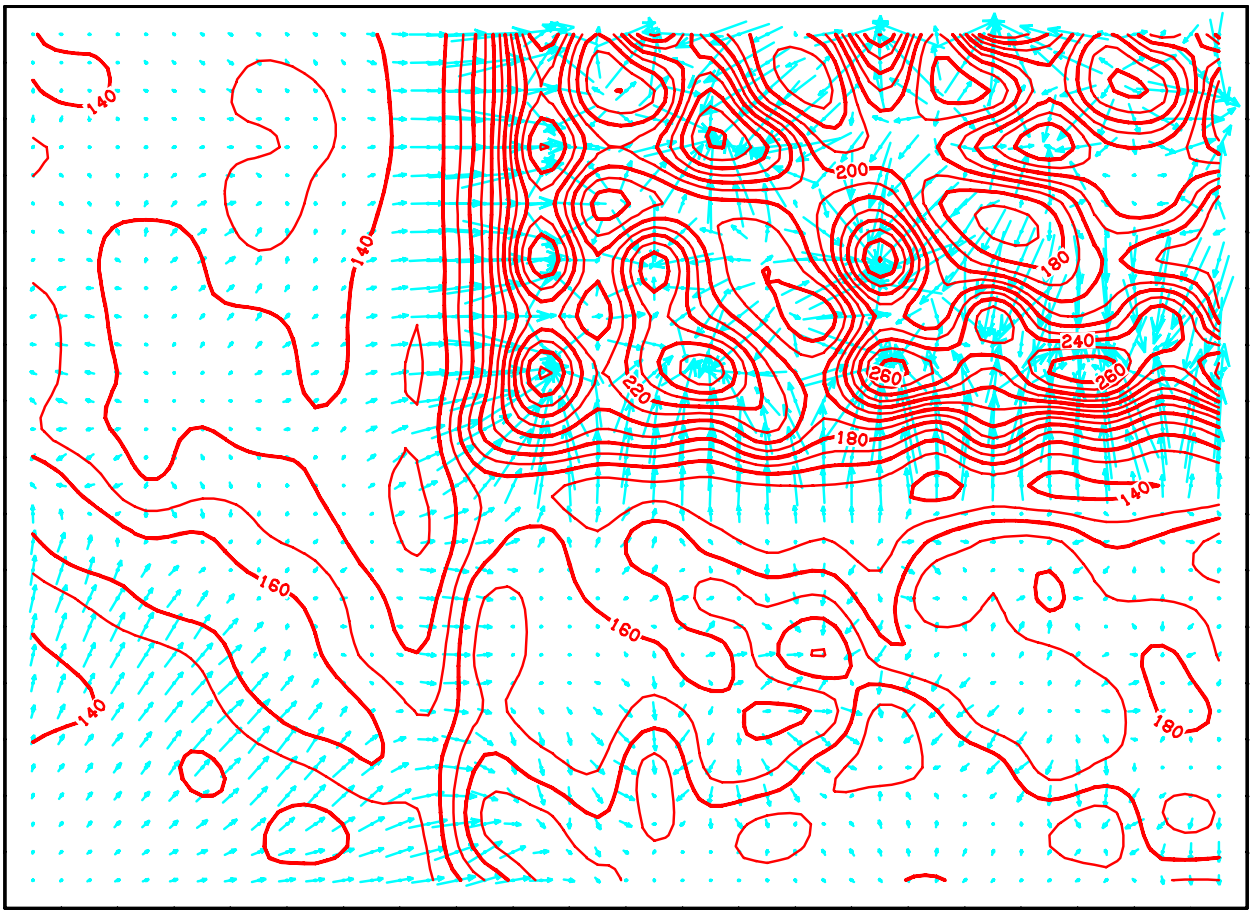

Figure 9c: Isotherms (red lines) and flow vectors (blue) in the vertical x-y plane k=3.

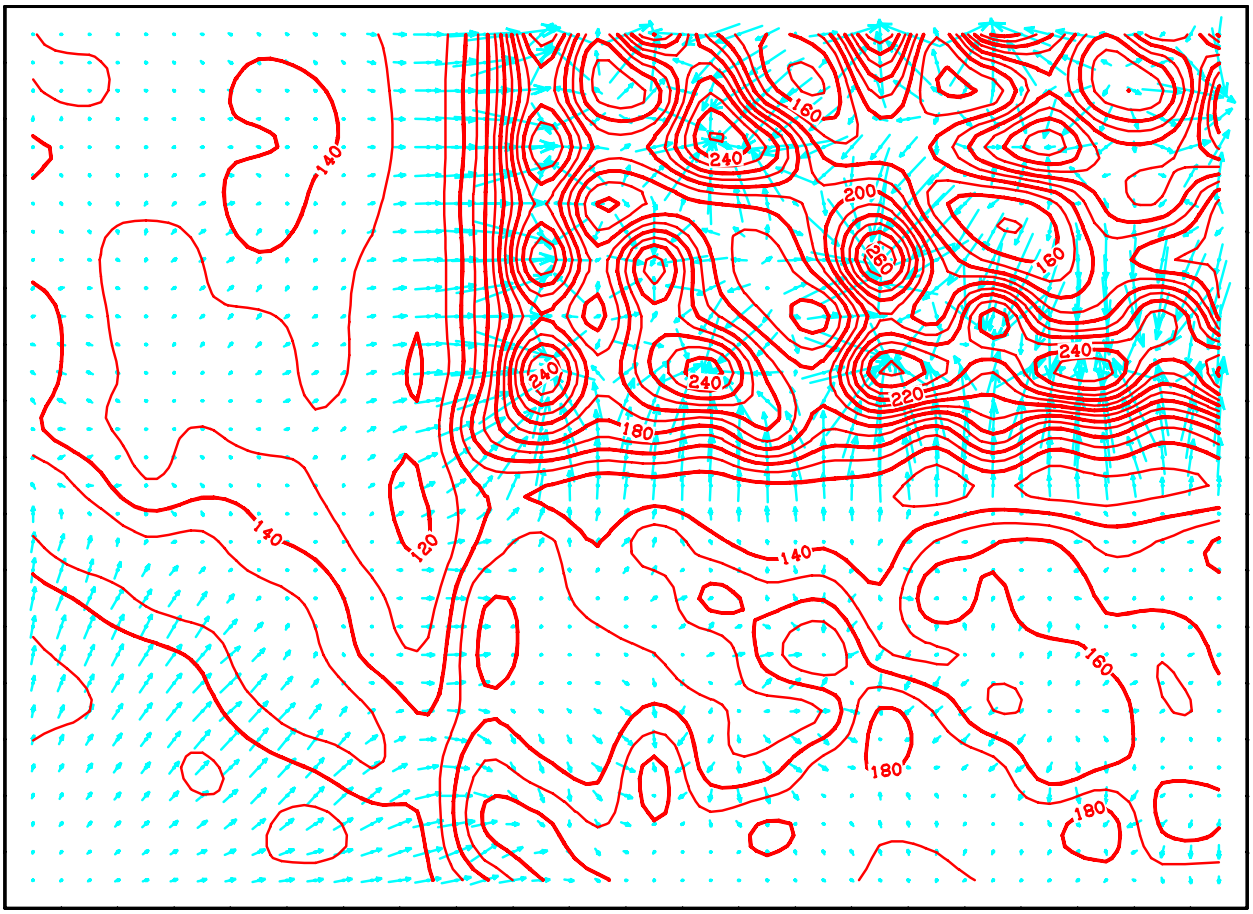

Figure 9d: Isotherms (red lines) and flow vectors (blue) in the vertical x-y plane k=4.

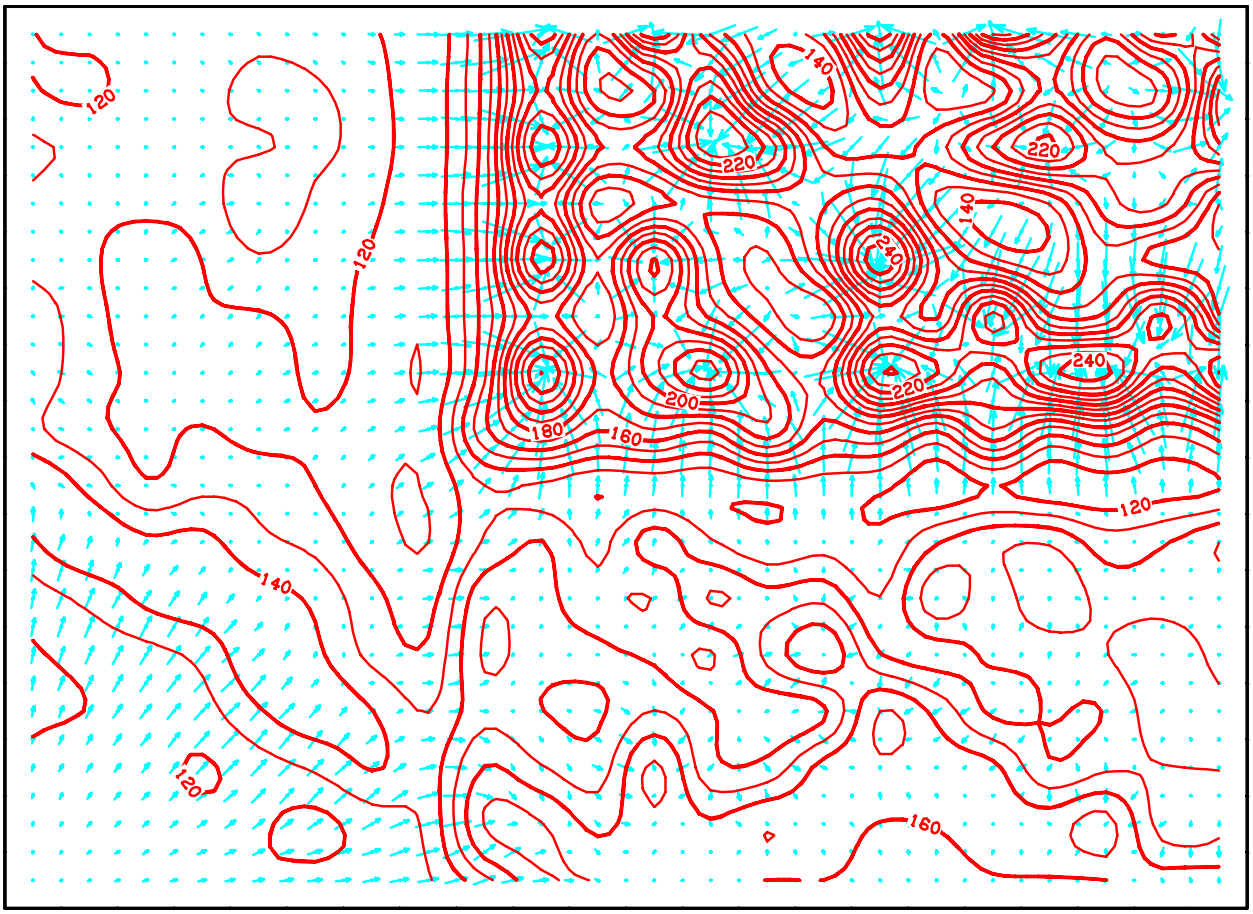

Figure 9e: Isotherms (red lines) and flow vectors (blue) in the vertical x-y plane k=5.

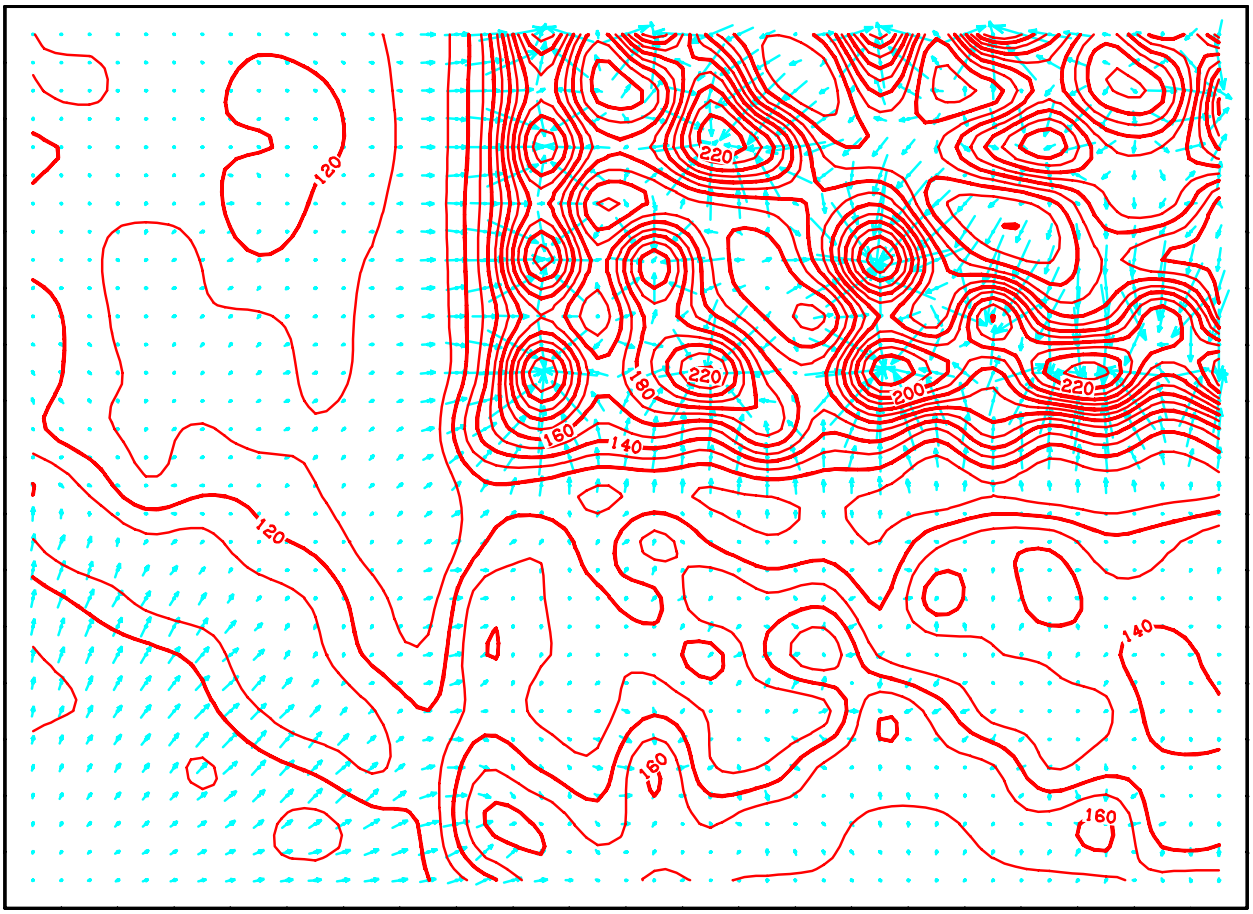

Figure 9f: Isotherms (red lines) and flow vectors (blue) in the vertical x-y plane k=6.

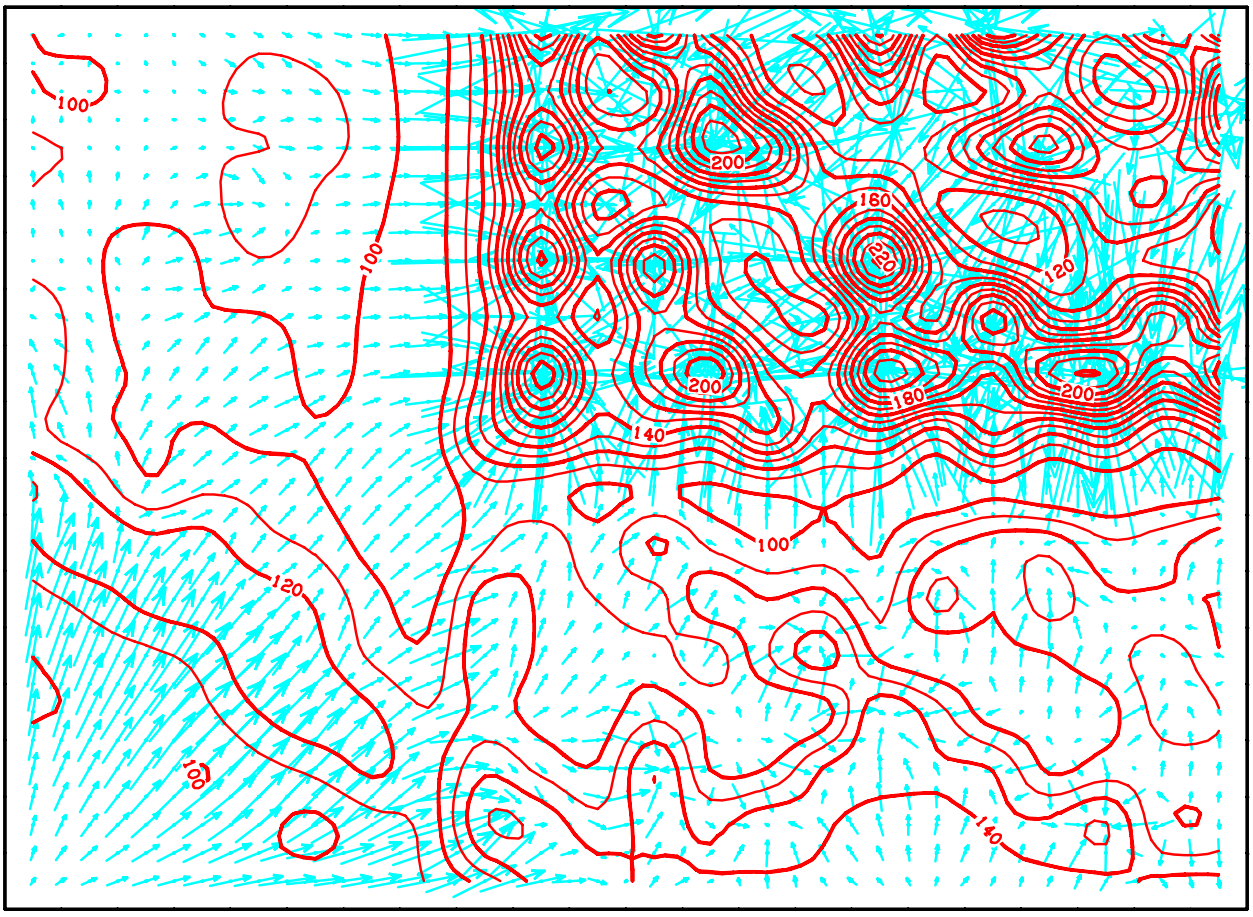

Figure 9g: Isotherms (red lines) and flow vectors (blue) in the vertical x-y plane k=7.

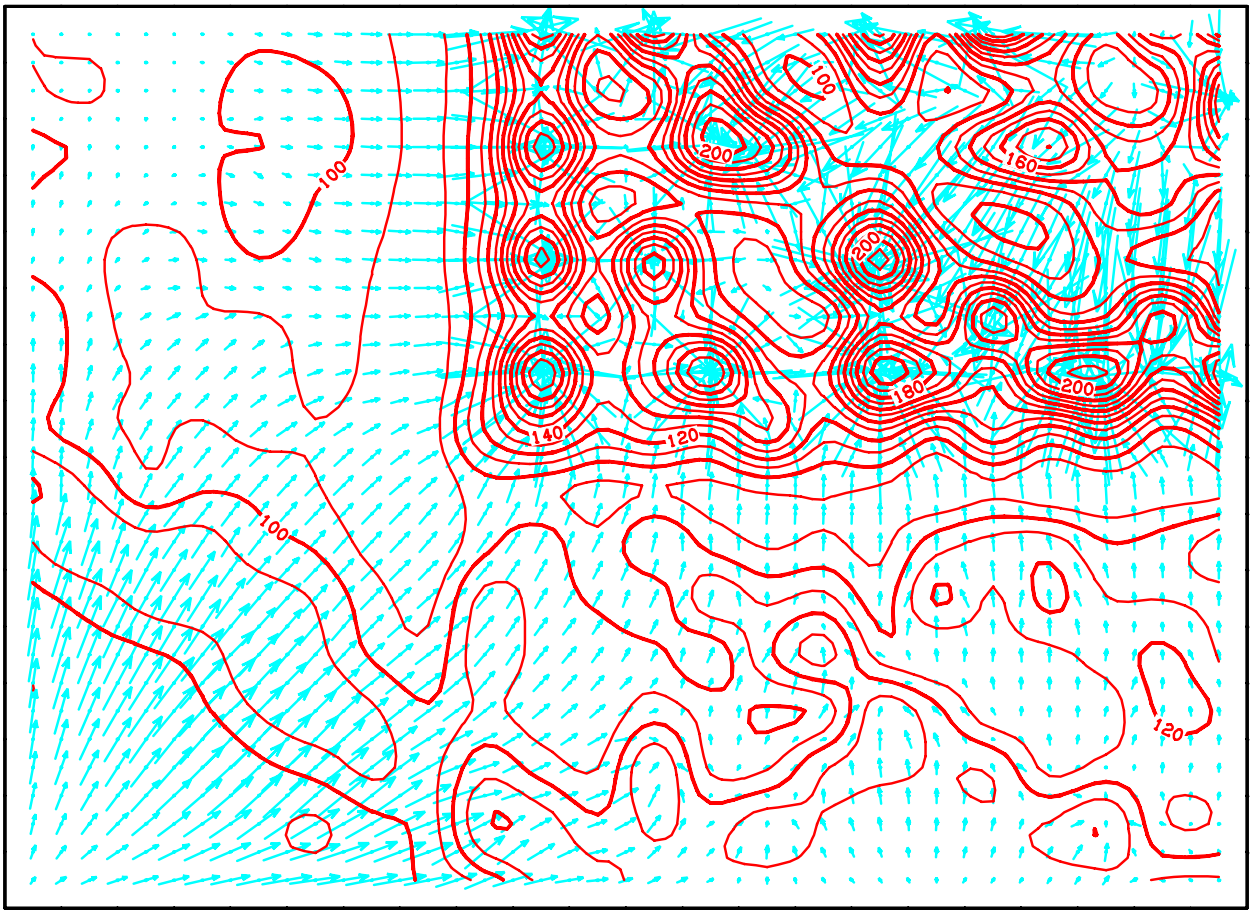

Figure 9h: Isotherms (red lines) and flow vectors (blue) in the vertical x-y plane k=8.

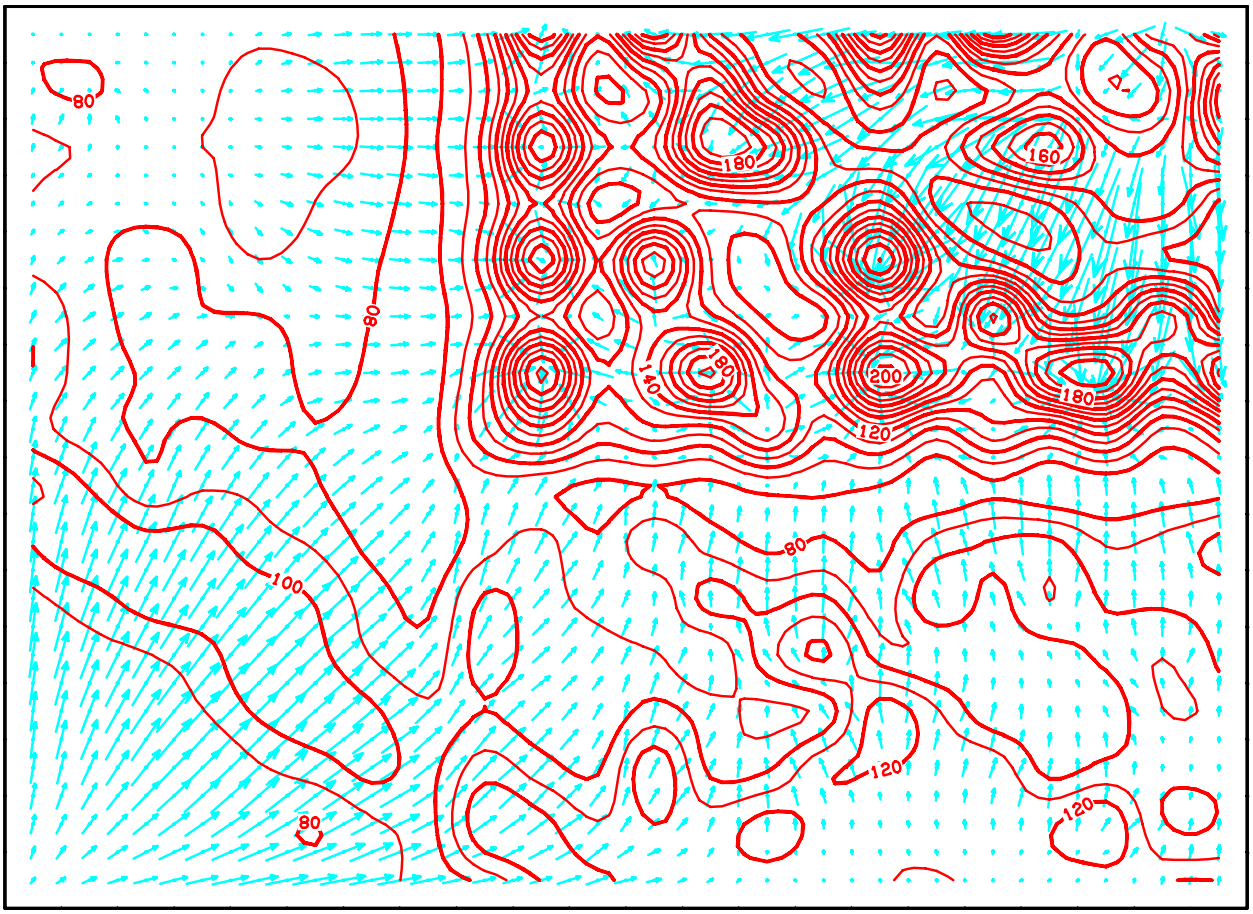

Figure 9i: Isotherms (red lines) and flow vectors (blue) in the vertical x-y plane k=9.

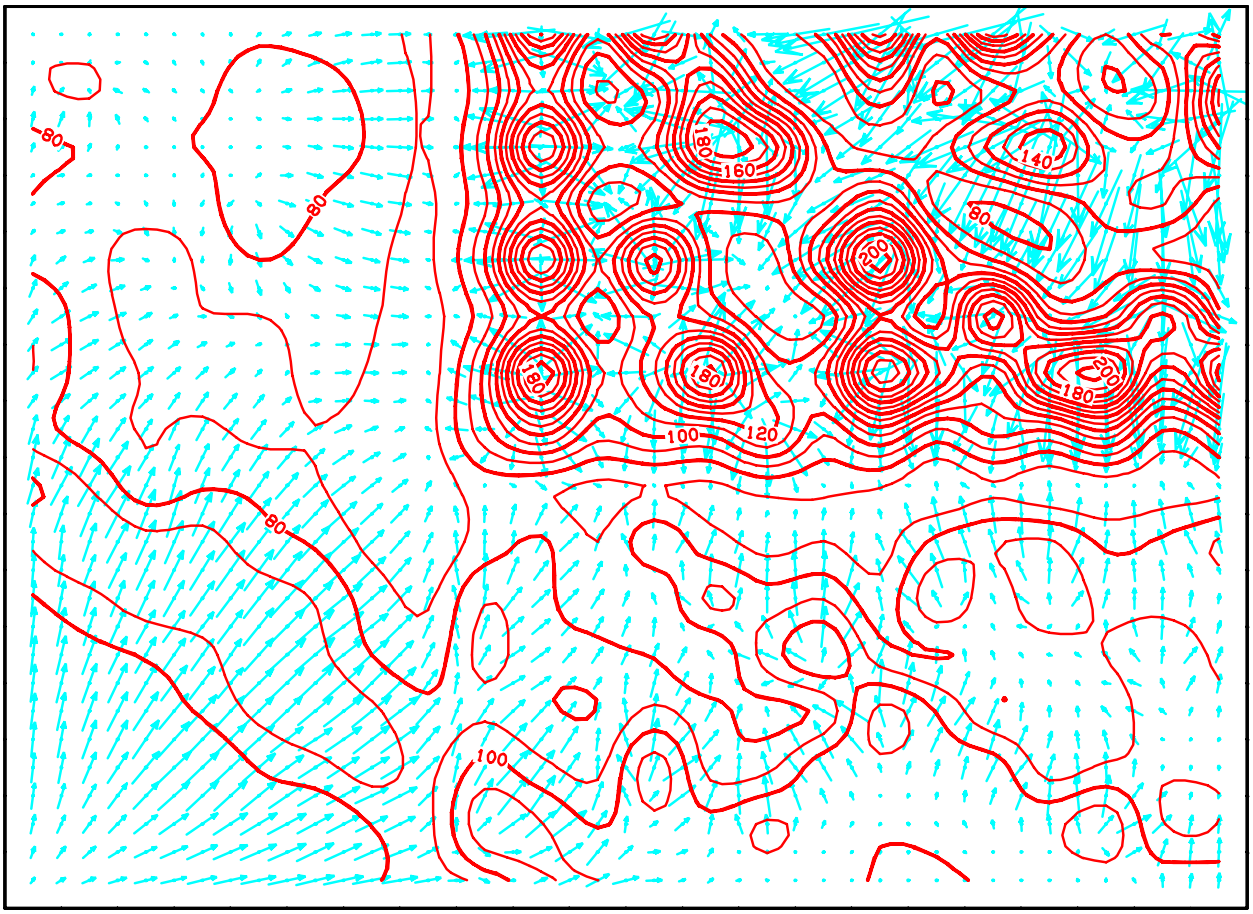

Figure 9j: Isotherms (red lines) and flow vectors (blue) in the vertical x-y plane k=10.

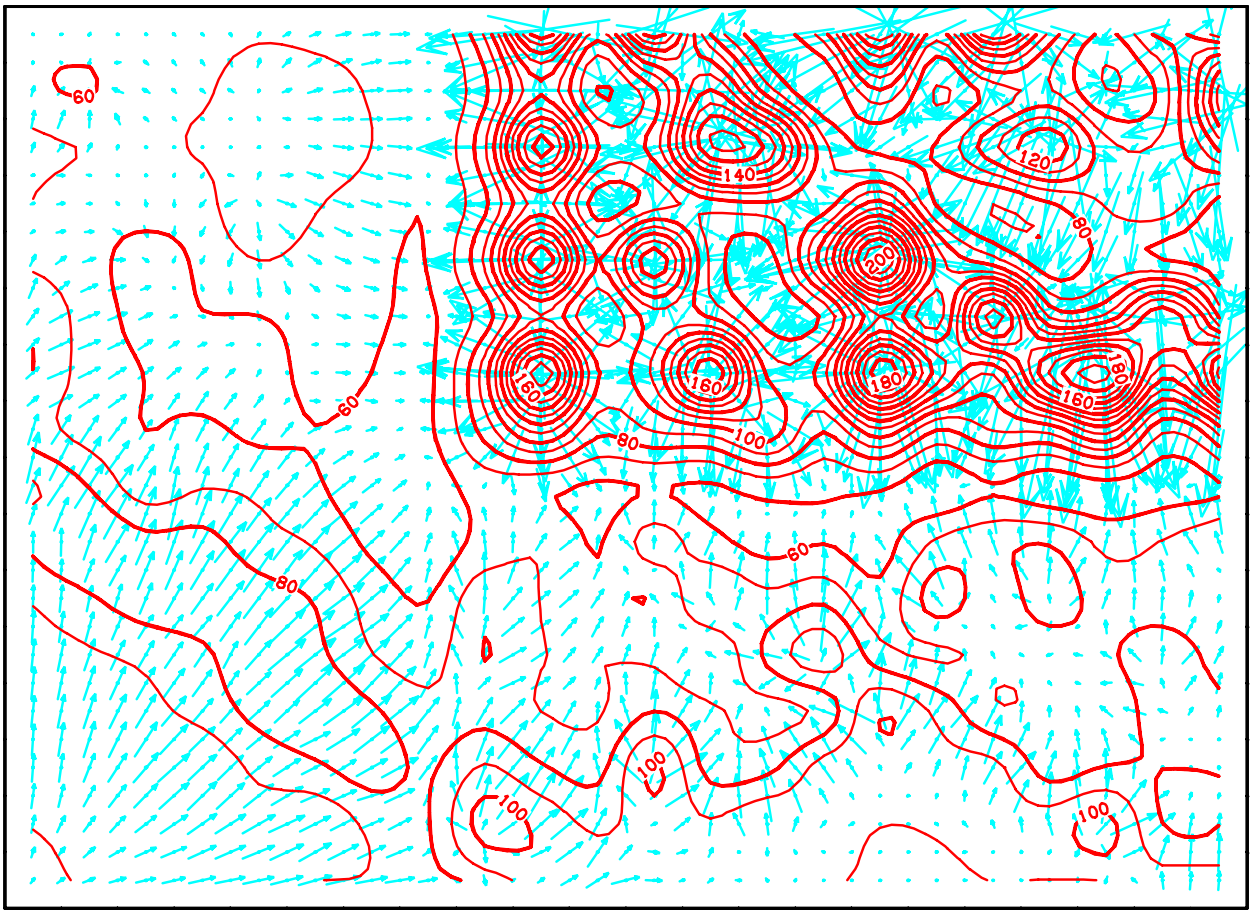

Figure 9k: Isotherms (red lines) and flow vectors (blue) in the vertical x-y plane k=11.

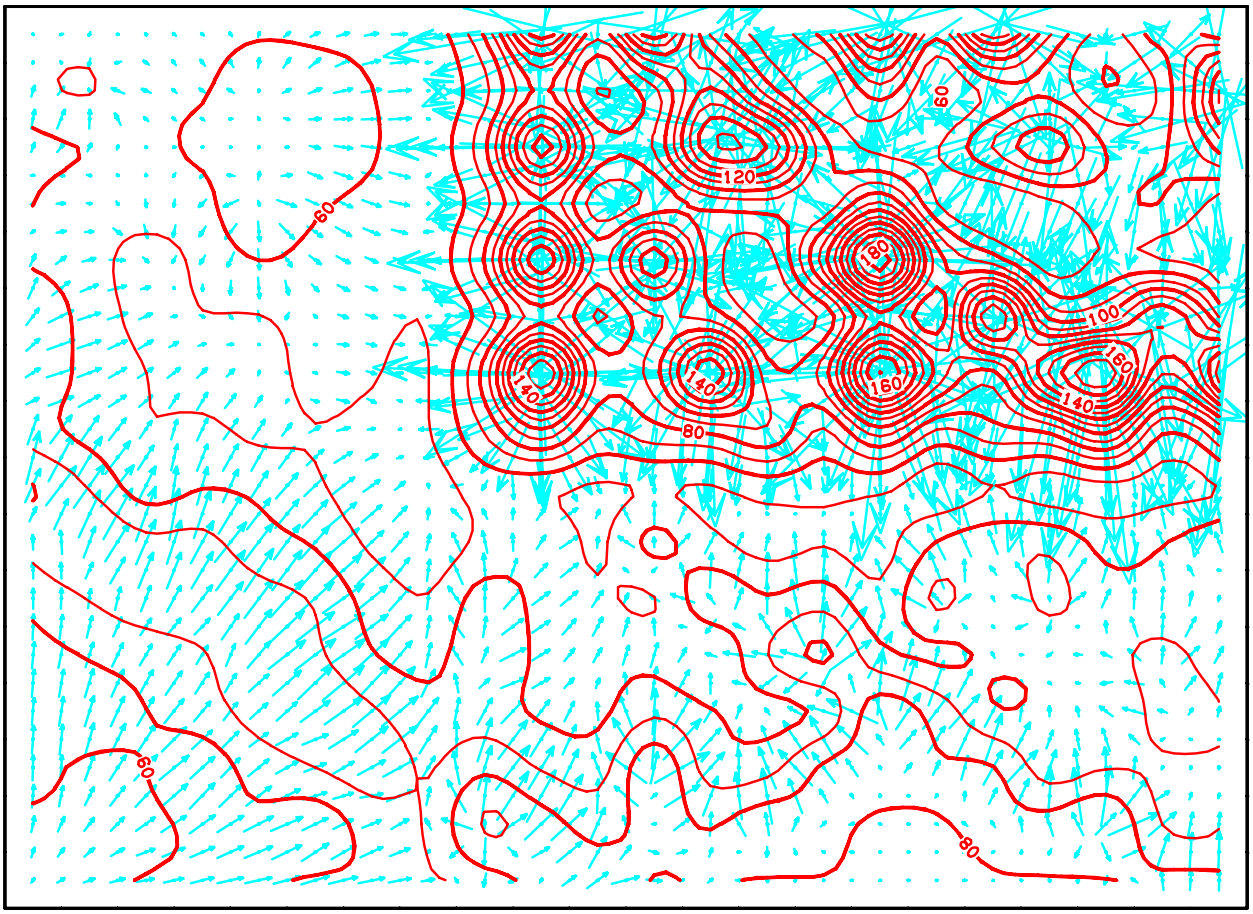

Figure 9l: Isotherms (red lines) and flow vectors (blue) in the vertical x-y plane k=12.

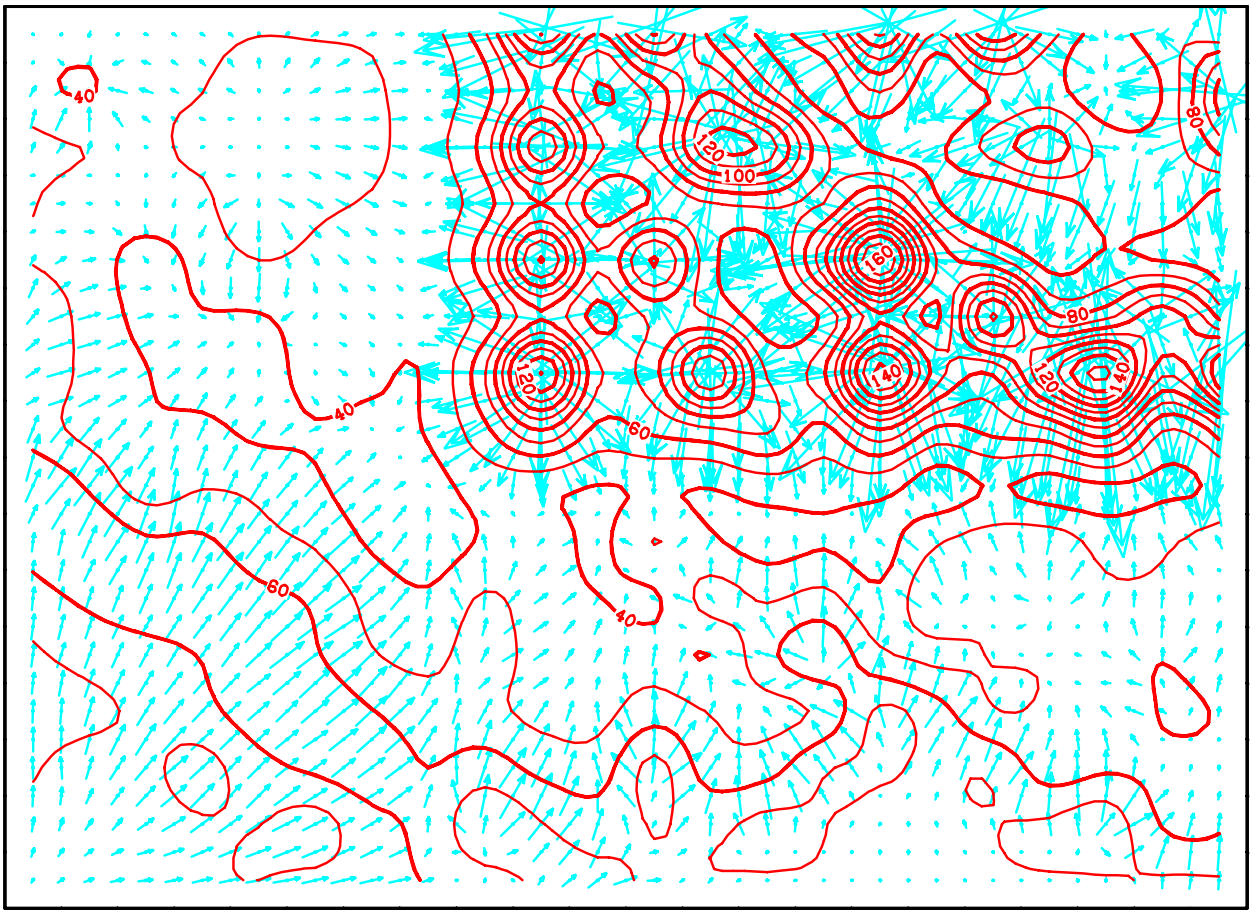

Figure 9m: Isotherms (red lines) and flow vectors (blue) in the vertical x-y plane k=13.

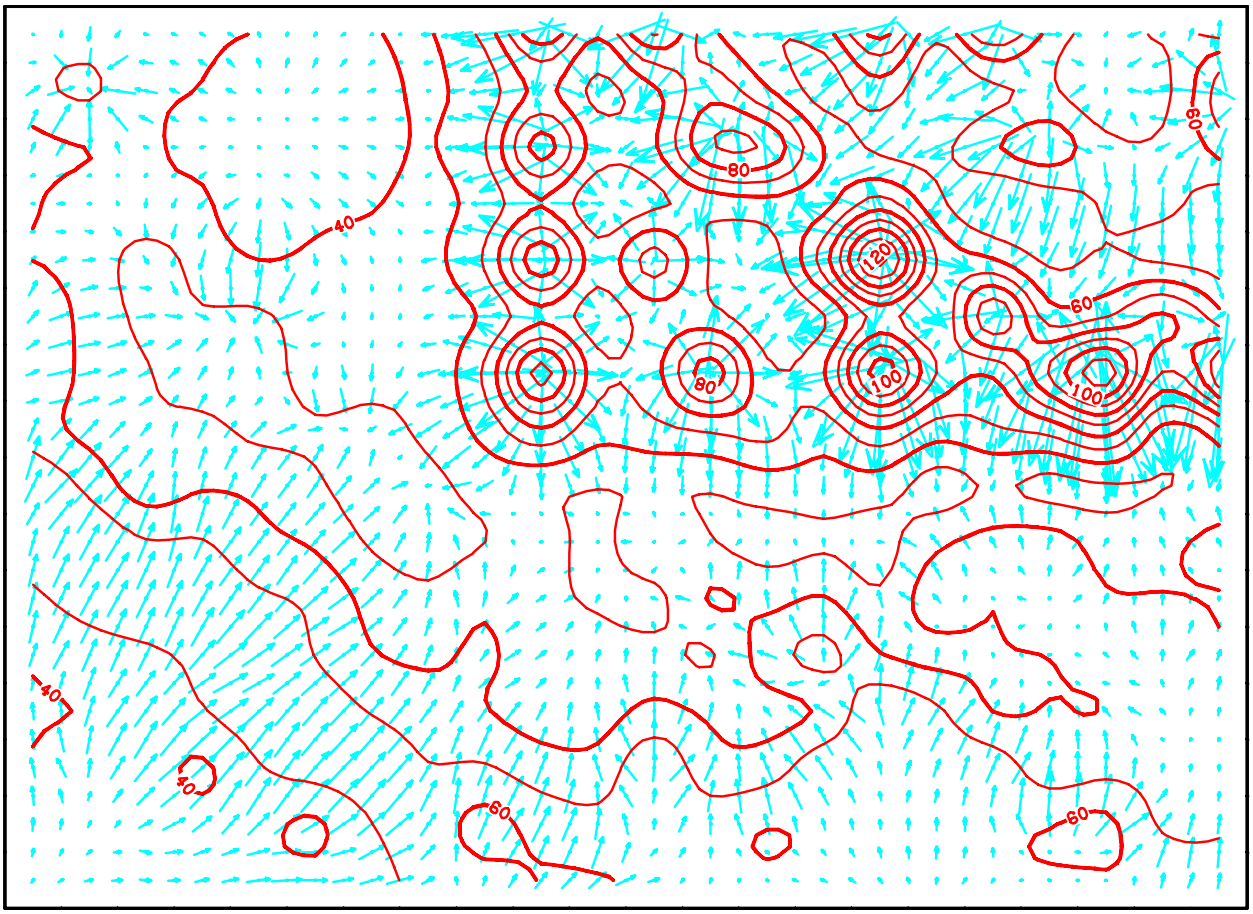

Figure 9n: Isotherms (red lines) and flow vectors (blue) in the vertical x-y plane k=14.

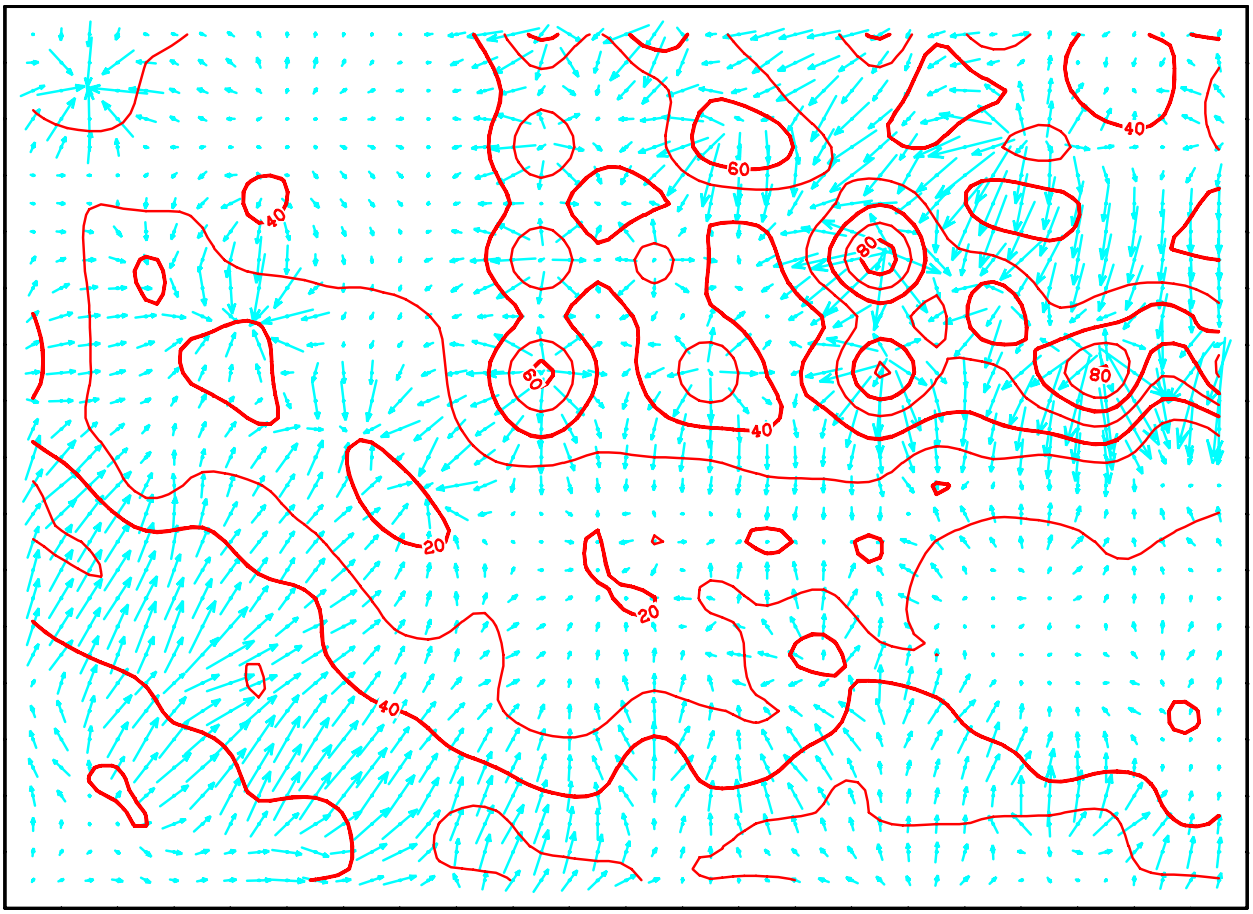

Figure 9o: Isotherms (red lines) and flow vectors (blue) in the vertical x-y plane k=15.

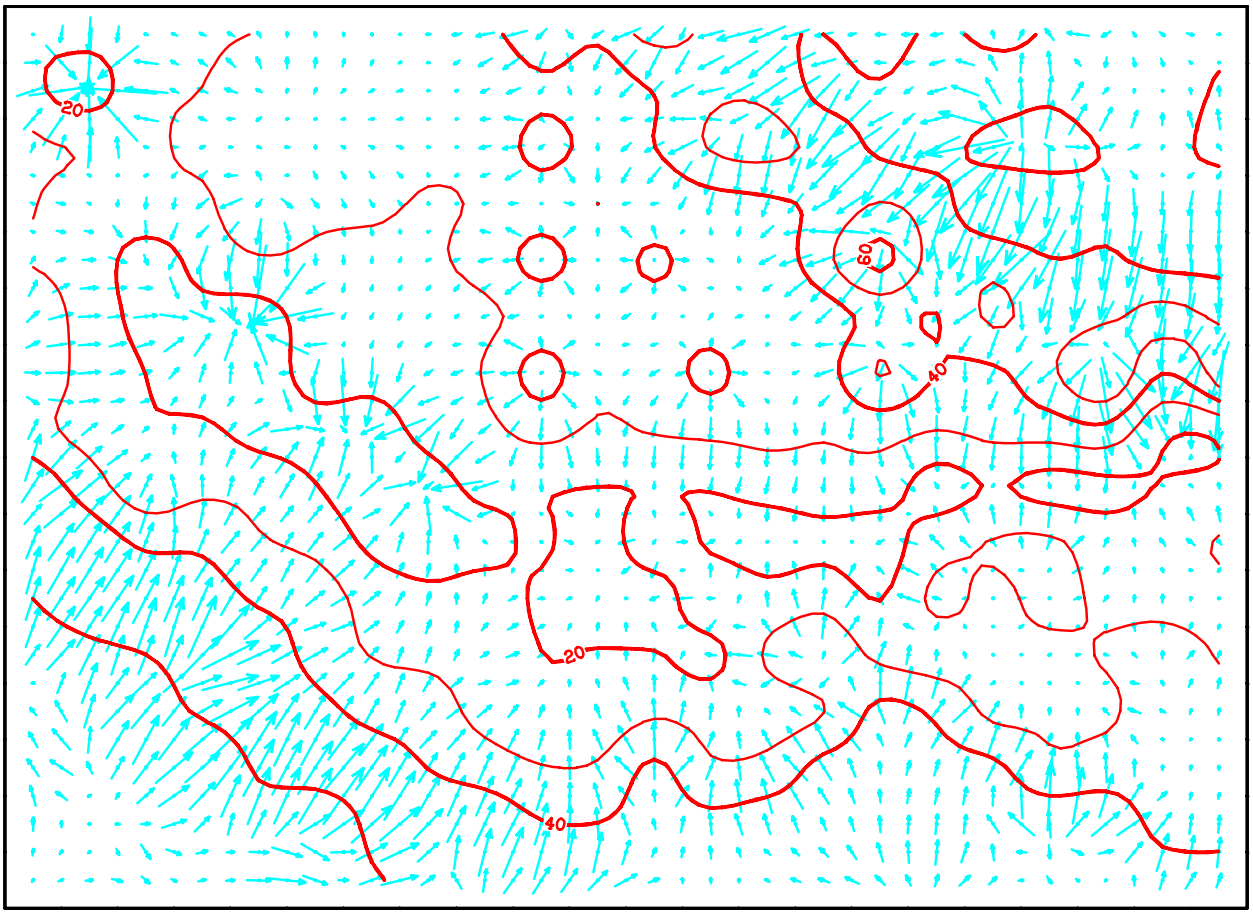

Figure 9p: Isotherms (red lines) and flow vectors (blue) in the vertical x-y plane k=16.

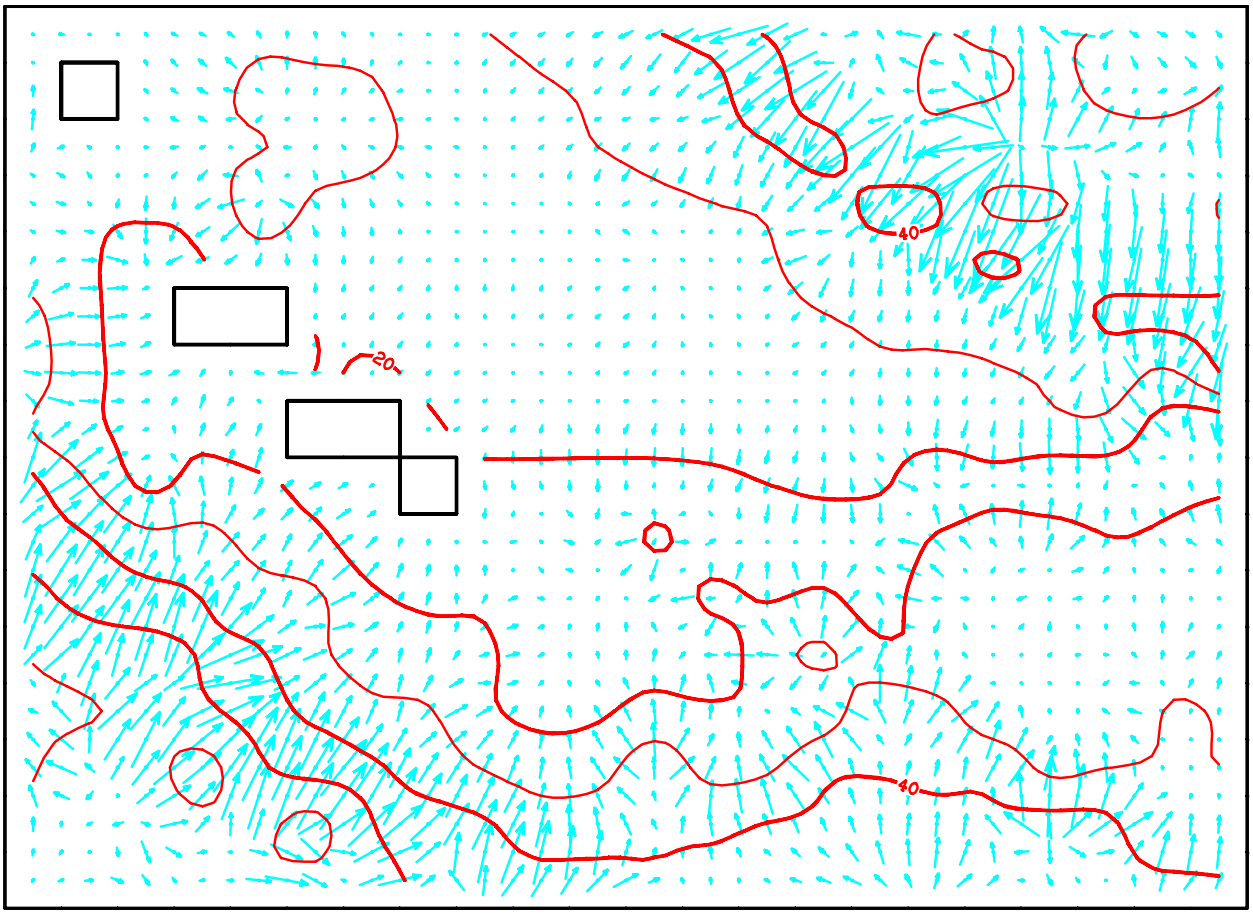

Figure 9q: Isotherms (red lines) and flow vectors (blue) in the vertical x-y plane k=17. Black boxes within the figure indicate void grid blocks.

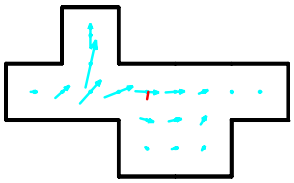

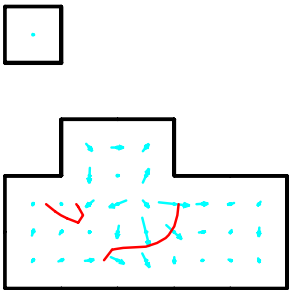

Figure 9r: Isotherms (red lines) and flow vectors (blue) in the vertical x-y plane k=18. Most of this layer contains void grid blocks.

VI. Future Work

The preceding sections present a preliminary 3-D natural state model for the Mountain Home geothermal prospect. The model was conditioned using the available temperature data from five (5) deep wells in the area. In Phase II and subsequent years, the model will be improved in several ways. A particularly simple representation of lithology was used in the preliminary model, and horizontal permeability distribution is poorly constrained. Results from ongoing analyses of faults and lithology will be helpful in improving these aspects of the preliminary model. An MT survey is planned for Phase II; results from this survey are expected to provide additional information on permeability distribution in the area. At present, no pressure data are available, and it is not known if the computed pressures correspond to reality. Acquisition of reliable pressure data will require access to deep wells; such access is also required for well tests designed to measure subsurface permeability distribution. The model will no doubt evolve as additional data become available.

VII. References

Pritchett, J.W. (2011), STAR User's Manual Version 11.0, Leidos Inc., San Diego, California, U.S.A.